THE MATHEMATICAL MODELS OF NUTRITIONAL PLASTICITY AND THE BIFURCATION IN A NONLOCAL DIFFUSION EQUATION

By

Yu Liang

A DISSERTATION

Submitted to
Michigan State University
in partial fulfillment of the requirements
for the degree of

Applied Mathematics - Doctor of Philosophy

2016

ABSTRACT

THE MATHEMATICAL MODELS OF NUTRITIONAL PLASTICITY AND THE BIFURCATION IN A NONLOCAL DIFFUSION EQUATION

By

Yu Liang

The thesis consists of two parts. In the first part, I investigate the developmental mechanisms that regulate the nutritional plasticity of organ sizes in *Drosophila melanogaster*, the fruit fly. Here I focus on the insulin-like signalling pathway (IIS) through which the developmental nutrition is signalled to growing organs. Two mathematical models, an ODE model and a PDE model, are established based on the IIS pathway. In the ODE model, the gene expression of each component in IIS pathway is considered as model variables. By analyzing the steady states of the ODE model under different parameter settings, the hypothesis that the difference of the nutritional plasticity among all organs of *Drosophila melanogaster* is due to the variation of the total gene expressions of components in IIS pathway is verified. Furthermore, the forkhead transcription factor FOXO, a negative growth regulator that is activated when nutrition and insulin signaling are low, is a key factor to maintain organ-specific differences in nutritional-plasticity and insulin-sensitivity. In the PDE model, I include the cellular structure and transportation within the cell. The transportation of proteins between the nucleus and the cell membrane is modelled with an advection-diffusion process. In simulations of the PDEs system, the hypothesis that the concentration of FOXO decreases as the concentration of insulin increase is verified.

In the second part of the thesis, I study the bifurcation properties of the nonlocal Chafee-Infante problem:

$$L_\epsilon u + \lambda(u - u^3) = 0.$$

Here, instead of the Laplacian, $L_\epsilon u$ is an integral defined by

$$L_\epsilon u = \int_0^\pi \epsilon^{-3} J(\frac{y-x}{\epsilon})(u(y) - u(x))dy,$$

where $J(x)$ is a continuous, non-negative, radially symmetric kernel with $J(0) > 0$. It is shown that as the scaling parameter ϵ approaches zero, the equation has pitchfork bifurcations at the eigenvalues of L_ϵ and these eigenvalues are close to those of $c_J\Delta$, with c_J constant. A concrete example is considered, and the bifurcation result is demonstrated by solving the equation with Newton's Method.

ACKNOWLEDGMENTS

I would like to express the deepest appreciation to my advisor, Dr. Peter Bates, for his guidance, assistance, encouragement, and hearty support in all the phases of my doctoral program at Michigan State University. This dissertation would not have been possible without his guidance and persistent help.

I would like to thank my committee members, Dr. Keith Promislow, Dr. Moxun Tang, Dr. Chichia Chiu for taking time to serve on my dissertation committee and for their useful comments and suggestions.

I am thankful to Dr. Alexzender Shingleton for valuable discussions, during which they provided me with inspiring suggestions about my research.

I am grateful to Ji Li, Jiayin Jin, Yin Cao, Qiliang Wu and many others for their friendship at Michigan State University.

At last, but by no means the least, my heart-felt appreciations go to my dearest families for their continuous and time-invariant support. Without their understanding, this work cannot be done.

TABLE OF CONTENTS

LIST OF FIGURES

Chapter 1

Introduction of the mathematical models of nutritional plasticity

One of the defining qualities of life is that organisms are able to respond to environmental stimuli, either developmentally, physiologically or behaviorally. This process, called phenotypic plasticity, underlies such diverse phenomena as the effect of developmental nutrition on adult body size in animals, the melanization of human skin in response to UV irradiation, and escape response to perceived predators in animal prey. An important aspect of phenotypic plasticity is that the degree of the response is appropriate to the degree of the stimulus. A poor match between stimulus and response can have severe implications for organismal form and function. For example, in humans anaphylaxis results from an inappropriately severe reaction to allergens. Conversely, type 2 diabetes is a result of a reduced response to circulating sugars in the blood stream. Work over the last 50 years has revealed myriad signaling pathways that transduce environmental information to developmental, physiological or neurological processes. Nevertheless, whilst we have a good understanding of the components of these pathway, the factors that regulate whether a signaling pathway amplifies or attenuates variation in an environmental signal are less well elucidated. More generally, we have a poor understanding of how organisms and the cells within them are able to manipulate signal transduction pathways to regulate the degree of response to environmental change.

Due to the innate complexities of signaling pathways, a fruitful approach to understanding how they amplify or attenuate environmental signals is to model them in silico. These models can be used to explore how changes in pathway structure and function affects how the pathway transduces environmental information. The resulting hypotheses can then be tested in vivo, in model organisms where genetic engineering allows precise manipulation of the signaling pathway. The insulin/IGF-signaling (IIS) pathway is an ideal system with which to explore the function of signaling pathways that underlie phenotypic plasticity (here referred to as plasticity pathways). In developing animals the IIS pathway regulates growth and development in response to nutrition. In adult animals the IIS pathway regulates, among other things, the uptake of sugars from the blood stream (in vertebrates) or hemolymph (in arthropods). In mammals, these metabolic and mitogenic processes are mediated by the insulin receptor and the insulin-like growth factor (IGF) receptors, respectively. In contrast, arthropods such as Drosophila have a single insulin receptor. Nevertheless, all insulin/IGF receptors feed into the same pathway, which is extremely conserved among all animals and has been well elucidated. Briefly, insulin-like peptides (ILPs) are released into the blood stream or hemolymph in response to developmental nutrition. These peptides then bind to the insulin receptor on the cell membrane and initiate a signal-transduction cascade that ultimately regulates the expression of genes that, when translated into proteins, regulate cell growth, proliferation and metabolism. In developing animals, a reduction in nutrition reduces signaling through the pathway, which in turn initiates the transcription of growth inhibitors. The result is a reduction in cell growth and proliferation leading to a decrease in final organ and body size. Importantly, not all organs show the same growth response to changes in developmental nutrition and IIS. In the fruit fly, *Drosophila melanogaster*, a reduction in developmental nutrition has more of an effect on wing size than on genital size, and this is a consequence of genital growth being less sensitive to changes in IIS. Similarly, in mammals the developing brain is relatively insensitive to changes in

nutrition, a phenomenon called head sparing. Such organ-specific differences in nutritional- and insulin-sensitivity is fundamental to ensure that final body proportion is correct across a range of adult sizes.

Work on Drosophila has revealed that the reduced insulin-sensitivity of the genitalia is a consequence of changes in the expression of key genes in the IIS pathway, specifically the forkhead transcription factor FOXO, a negative growth regulator. When IIS is high, FOXO is phosphorylated by the IIS pathway. This disrupts DNA binding and causes FOXO to translocate to the cytoplasm. A decline in IIS leads to de-phosphorylation of FOXO, which accumulates in the nucleus and initiates the transcription of growth inhibitors, as well as the insulin receptor itself. The genitalia of Drosophila are able to limit their size response to changes in nutrition and IIS by expressing only low levels of FOXO. Consequently, a decline in developmental nutrition does not result in the activation of growth inhibitors in the genitalia, allowing them to maintain growth even as the growth of other organs and of the body as a whole is slowed.

These studies demonstrate that changes in the expression or activity of genes within plasticity pathways can affect whether they amplify or attenuate variation in an environmental signal. What is unclear is the generality of this finding. Do changes in expression/activity of other components in the pathway have the same effect? How do feedback loops within the plasticity pathway affect how it transduces the environmental signal? Can we make broad generalizations as to how changes in a plasticity pathways structure and function changes sensitivity of phenotype to environmental signals? In this dissertation, we establish the mathematical models of the insulin-like signaling pathway, which serve as the fundamental tools for exploring the mechanisms regulating the nutritional plasticity of organs in Drosophila melanogaster.

Chapter 2

Backgrounds

2.1 Size and shape in insects

Intuitively, individuals with larger bodies tend to have larger constituent parts. For instant, larger humans will have longer arms and legs, bigger livers and larger hearts. Bigger fruit flies tend to have larger wings and legs. This scaling relationship between the sizes of individual traits and the size of the whole body is called allometry ([13]). Allometries are traditionally modelled using the allometric equation $y = ax^b$, where x and y are two given traits. A Log-transformation of this equation produces the linear equation $\log(y) = \log(a) + b\log(x)$, i.e., a linear relation between the log of trait size x and the log of trait size y. Furthermore, the slope of the linear relation is represented by the real number b. Thus, we are able to classify the allometries according to the value of b. We say that two traits scale isometrically when $b = 1$. This is the case of palp size against body size in D. melanogaster (see fig 2.1). Trait y scale hypometrically to trait x when $b < 1$, which is the case of genital size against body size in *Drosophila melanogaster* in fig 2.1. Trait y scale hypermetrically to trait x when $b > 1$.

Allometry not only describes the scaling relationship between traits and body, but also the scaling relationship among traits themselves. Generally, it is defined by the proportional change in the dimensions of one trait relative to another trait or to overall body size. More specifically, there are three types of allometries: ontogenetic, evolotionary, and static allometries. Ontegenetic allometries describe the growth trajectories within a single individual. They characterize the growth of

an organ relative to the growth of another organ or growth of the body in a single individual. Evolutionary allometries describe the relative size of different organs among individuals at the same developmental stage across species. Static allometries are similar to evolutionary allometries but they describe the relative size of different organs within species. While the variation of growth in evolutionary allometries is caused by the evolving of different species in the evolutionary process, the variation of growth in static allometries may due to the genetic difference between individuals, the difference in the environment in which they developed or due to the interaction between the two. Hence, the mechanisms behind the static allometries according to genetic and environmental factors are very different. Furthermore, both the genetic and environmental factors could generate various allometric relationships due to the different sources of those genetic and environmental factors. For instance, temperature, nutrition, sunlight, etc, are different environmental factors that could contribute to the static allometries. Similarly, there may be different sources of genetic variation, such that allelic variation at one locus may produce a different allometries than variation at another. This suggests that researchers should investigate different biology mechanisms in regards to any specific factor of the static allometries. In this dissertation, we mainly focus on investigating the mechanisms related to the environmental static allometries, especially for static allometries due to the nutritional variation. We eliminate the genetic factors by reproducing *Drosophila melanogaster*, fruit fly, with the same genotype in the lab and study any environmental factors by controlling the environment where the fruit flies are raised.

Environmental factors affect the static allometries because they regulate the rate and duration of cell growth and division. The developmental response to the environment is called phenotypic plasticity. The response of trait size against the value of a particular environmental variable for a single genotype is the reaction norm. It describes the pattern of phenotypic variation produced by a single genotype reared under a range of environmental conditions. For instance, malnutrition

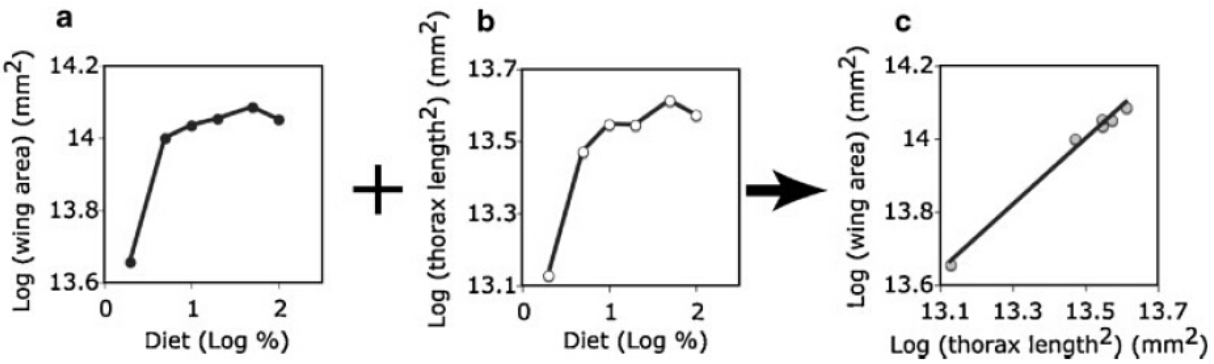

Figure 2.1: The relationship between reaction norms and allometries.

during development reduces final adult size in *Drosophila melanogaster*. Fig 2.1 a and b show the reaction norms for wing area and thorax length of *Drosophila melanogaster* as a function of larval nutrition. Combining fig 2.1 a and b, we get the nutritional static allometries between wing area and thorax length. ([13]) Hence, the environmental static allometries of two traits are directly related to the reaction norms of the two traits with respect to an environmental variable.

As one of the typical holometabolous insects, *Drosophila melanogaster* begin life as worm-like larvae, molting through three larval instars before undergoing complete metamorphosis as pupa and eventually closing into their adult form, shown in fig 2.2. Adult flies have a stiff exoskeleton and so they cannot continue to grow. Hence, adult body size is entirely regulated by growth during the premetamorphic larval stages. Further, the adult organs of *Drosophila melanogaster* are not visible until after metamorphosis. In fact, they grow as imaginal discs within the developing larvae, each disc corresponding to an adult structure. During metamorphosis their imaginal discs differentiate and evaginate to form the adult organs. Thus, the adult organ size is also determined by growth of the imaginal discs during the larval stages. Those physiological processes controlling the metamorphosis of *Drosophila melanogaster* are regulated by several hormones. At some point in the final larval instar, attainment of a particular body size is associated with a reduction in the levels of circulating juvenile hormones. This size is called the critical size. Once critical size is attained,

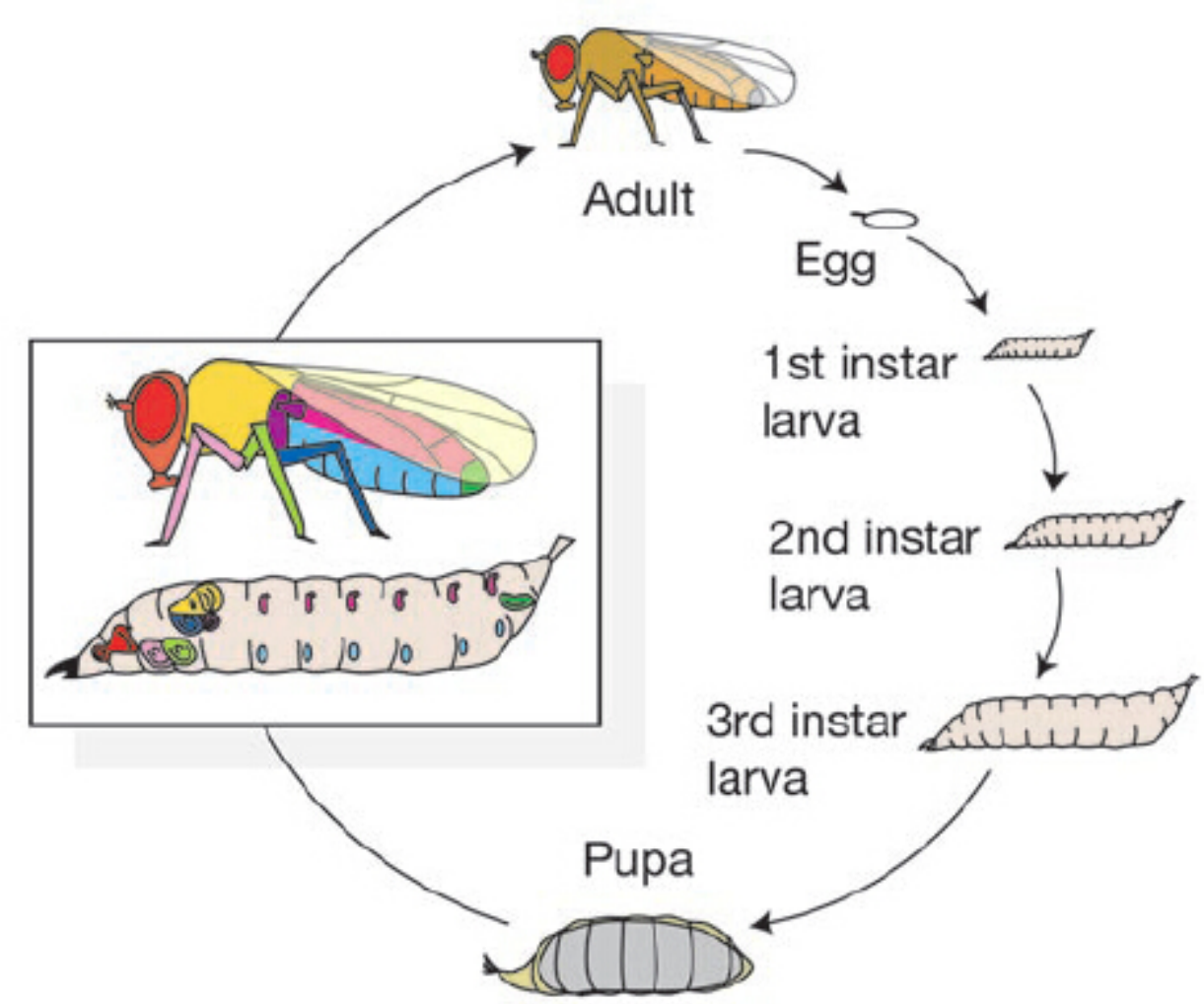

Figure 2.2: The life cycle of *Drosophila melanogaster*.

a larva irreversibly initiates the hormonal cascade that ends in metamorphosis, and so there is a delay between the attainment of critical size and the termination of body growth. This period is referred to as the terminal growth period (TGP). Thus, we have the following formulas about the final body or organ size of *Drosophila melanogaster*:

$$F = CS + R\delta t,$$

where F is the final body or organ size, CS is critical size, R is the rate of growth during TGP and

δt is the duration of TGP.

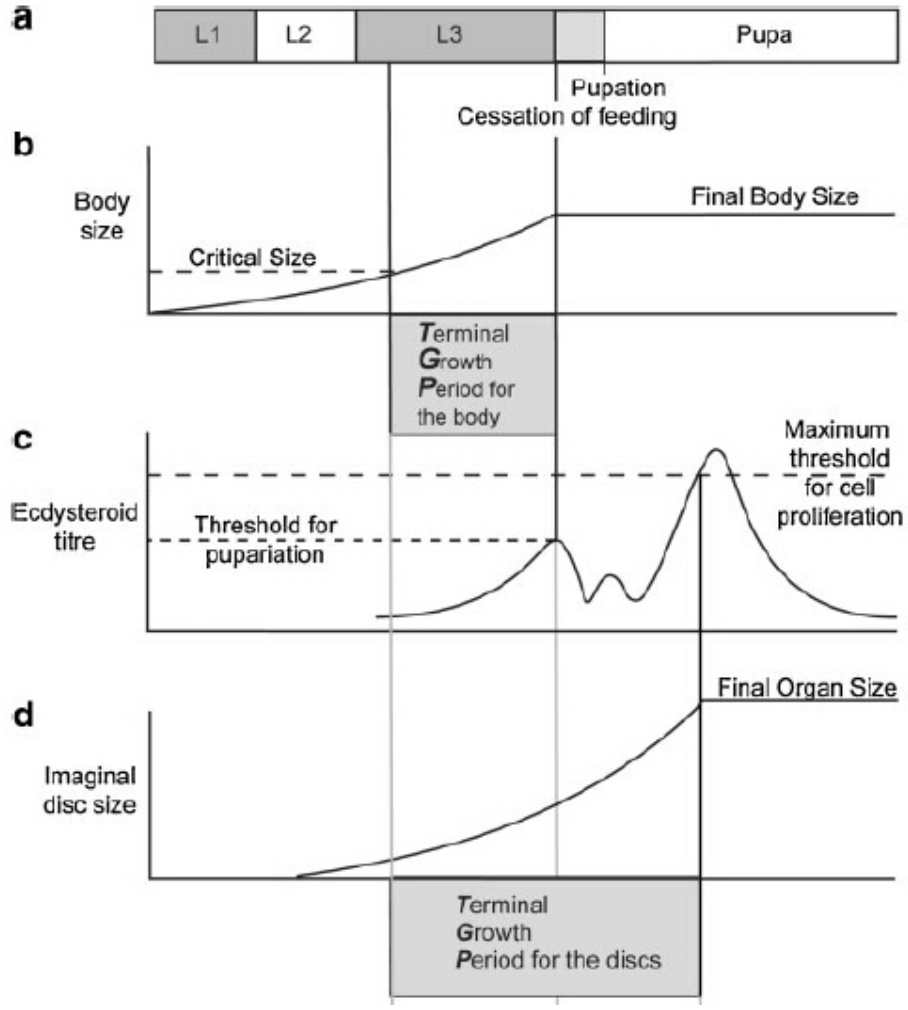

Figure 2.3: The nutritional regulation of body and organ size in *Drosophila melanogaster*.

2.2 The insulin signaling pathway

The final body and organ sizes in all animals vary when the developmental nutrition changes. In *Drosophila melanogaster* particularly, the growth response to nutrition is mediated through several inter-connected hormonal systems. One of them is through the release of dILPs in the brain.([12]) The insulin-like signaling pathway (IIS) system is comprised of three pathways (fig 2.4): the IIS pathway; the Target of Ramapmycin (TOR) signaling pathway, and the AMP-dependent kinase

(AMPK) pathway. These pathways are extremely conserved among all animals, and are essnetially identical in *Drosophila melanogaster* and vertebrates. However, in *Drosophila melanogaster* the metabolic and mitogenic roles of IIS, which in vertebrates are separated into insulin-like and growth-factor signaling respectively, are combined into a single pathway with a single insulin-receptor (InR). A reduction in dILP production causes a reduction in body and organ size, while increasing the cencentration of dILPs casuses an increase in body and organ size.

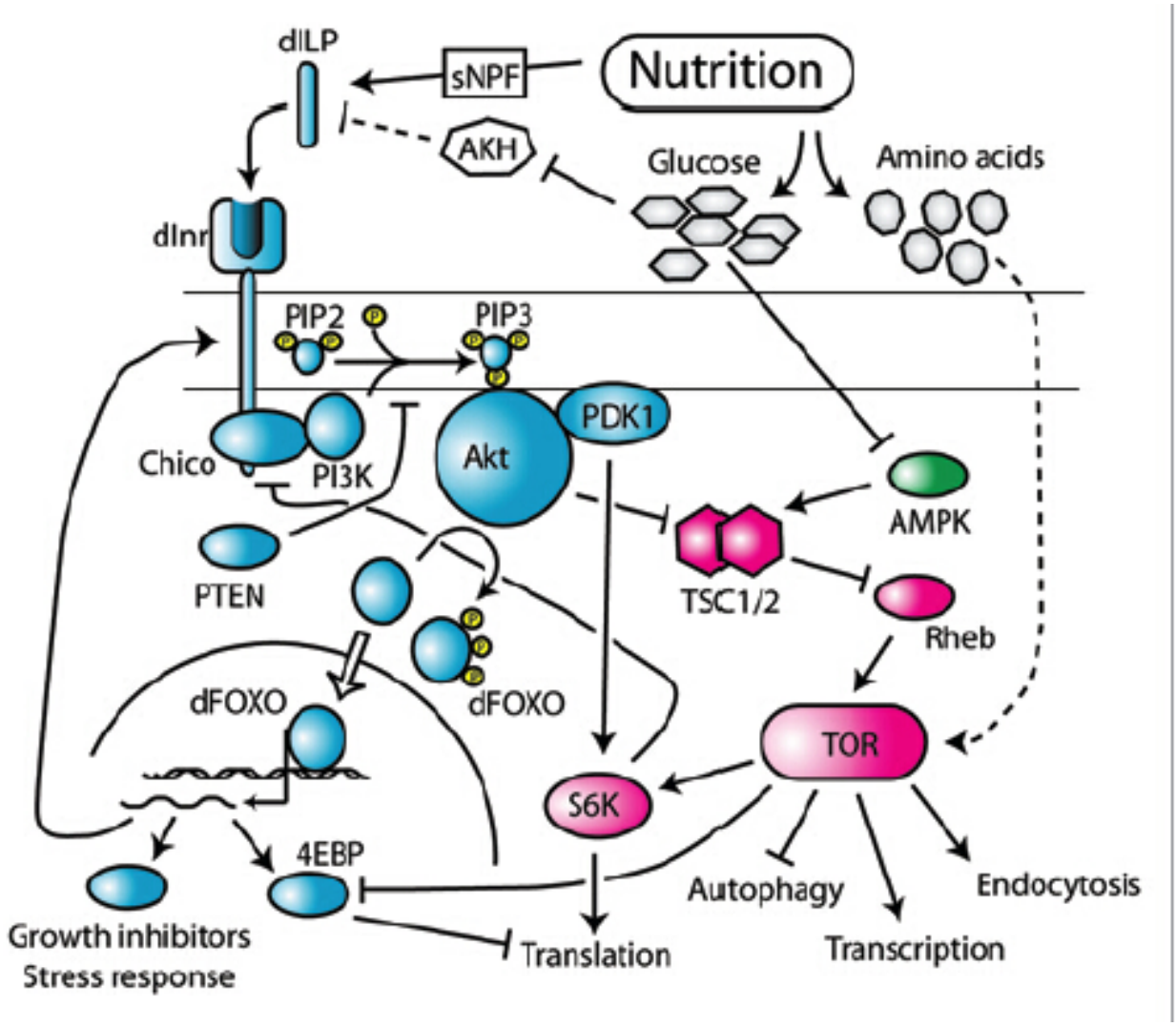

Figure 2.4: The IIS and TOR-signaling pathway in *Drosophila melanogaster*.

The freely diffusing dILPs molecules circulate in the extracellular fluid of *Drosophila melanogaster*,

where they bind to insulin receptors (InR) located on the cellular membrane of dividing cells. Binding of dILP to Inr results in receptor autophosphorylation. The receptor may then either bind a second dILP, which does not affect its phoshphorylation state, or may dissociate from the first dILP, which causes dephosphorylation. The dInr molecule may also be dephosphorylated by protein tyrosine phosphotases (PTP). Membrane-bound phosphorylated receptors can be reversibly internalized through endocytosis, where dephosphorylation by PTP releases them into the intracelluar pool of free InR. These free receptors can then be reversibly reintegrated into the cell membrane, where they become available to binding with dILPs. In addition to this recycling of InRs from the cell membrane, unphosphorylated receptors also enter the intracellular pool through synthesis and leave it through degradation. The phosphorylated InR recruits insulin receptor substrate (Chico) to the membrane and phosphorylates it, where upon it forms a complex with Pi3K. The resulting IRS-PI3K complex is an active protein kinase. The phosphorylated IRS-PI4K complex phosphrylates phosphatidylinostiol 4,5-bisphosphate, PI(4,5)P2 to PI(3,4,5)P3, at the cell membrane. Additionally, PI(3,4)P2 is converted to PI(3,4,5)P3 independently of IRS-PI3K. The Akt molecule binds to PI(3,4,5)P3 at the cellular membrane and activates the serine/threonine kinase Akt. Activated Akt detachs from the cell membrane and translocates to the nucleus (J. Cell Sci. 114, 2903-2910), where it phosphorylates the forkhead transcription factor FOXO. Transcriptional targets of FOXO include negative growth regulators, for example 4E-BP, as well as the insulin receptor Inr. Phosphorylation by Akt cause FOXO to translocate out of the nucleus and hence lose its transcriptional activity.

Chapter 3

A ODE model

3.1 Preliminary

To get a mathematical model of the IIS pathway including dFOXO, we develop an ODE system based on Sedaghat et la's model ([11]). We take Sedaghat et la's model with variables from x_2 to x_{17}, then include new variables for the activated and deactivated dFOXO. For better exploring our questions and modelling the reality of the pathway, we modify Sedaghat et la's model from several aspects. First, we add degradations for each of the complex in the pathway and include the basal transcriptions to the unphosphorylated states of insulin receptor, Chico, PI3K, Akt and dFOXO. Second, we model the lipids, Akt of the pathway by concentration instead of percentage. Third, a mathematical model of dFOXO subsystem is developed by the mechanism of the interaction of dFOXO and Akt. A positive feedback from activated dFOXO to insulin receptors is included in the model. Fourth, the relation between activity of PTPases and activated Akt is modeled by a smoothly exponential function instead of a linear function. The illustration of the new model about the IIS pathway is shown in figure 3.1.

Here we list the variables representing the molecules concentrations in the signalling pathway:

ILP:

I, concentration of insulin

InR:

$R_1(t)$, concentration of unbound unphosphorylated cell-surface receptors,

$R_2(t)$, concentration of once-bound unphosphorylated cell-surface receptors,

$R_3(t)$, concentration of phosphorylated twice-bound cell-surface receptors,

$R_4(t)$, concentration of phosphorylated once-bound cell-surface receptors,

$R_5(t)$, concentration of unbound unphosphorylated intracellular receptors,

$R_6(t)$, concentration of phosphorylated twice-bound intracellular receptors,

$R_7(t)$, concentration of phosphorylated once-bound intracellular receptors.

Chico:

$C_1(t)$, concentration of unphosphorylated Chico,

$C_2(t)$, concentration of phosphorylated Chico,

PI3K:

$\Phi_3(t)$, concentration of deactivated PI3K,

$\Xi(t)$, concentration of phosphorylated Chico-PI3K complex.

Lipids:

$P_3(t)$ be the concentration of $PI(3,4,5)P_3$,

$P_4(t)$ be the concentration of $PI(3,4)P_2$,

$P_5(t)$ be the concentration of $PI(4,5)P_2$.

Akt:

$A(t)$, concentration of deactivated Akt,

$A_p(t)$, concentration of activated Akt.

dFOXO:

$F(t)$, concentration of activated FOXO,

$f(t)$, concentration of deactivated FOXO.

PTP:

$P(t)$: A prefactor representing the relative activity of PTPases in the cell.

3.2 The Ordinary Differential Equations model of the IIS pathway

3.2.1 Insulin receptor subsystem

In the drosophila insulin receptors subsystem, each free drosophila insulin receptor could be potentially bound with two insulin. Unbound and bound insulin receptor cycle between cell membrane and cytoplasma. Bound insulin receptors on the cell membrane would phophorylate Chico and initiates a signal transduction cascade.

The synthesis of R_1: Free insulin receptors (R_1) on the membrane bind to insulin (I) and become once-bound unphosphorylated surface receptors (R_2) at the rate k_1. That reaction is reversible with rate k_{-1}. Phosphorylated once-bound surface receptors (R_4) are dephosphorylated by PTPases, release their insulin and become unbound unphosphorylated surface receptors (R_1) with rate $k_{-3}P$. At the same time, free surface receptors (R_1) pass through the cell membrane to become intracellular receptors (R_5) with rate k_4 and the intracellular receptors attach to the cell membrane, becoming surface receptors with rate k_{-4}. Finally, a certain fraction (d) of receptors degrade and are lost. Therefore, the synthesis rate of free receptor on the membrane, R_1, is expressed by

$$\dot{R_1} = -k_1 I R_1 + k_{-1} R_2 + k_{-3} P R_4 + k_{-4} R_5 - k_4 R_1 - d R_1. \tag{3.2.1}$$

The synthesis of R_2: In addition to the exchanges with R_1, described above, the once-bound unphosphorylated surface receptors (R_2) degrade at the same rate d and are phosphorylated to become phosphorylated once-bound surface receptors (R_4) at the rate k_3. Therefore, the synthesis

rate of R_2 is

$$\dot{R_2} = k_1 I R_1 - k_{-1} R_2 - k_3 R_2 - d R_2. \tag{3.2.2}$$

The synthesis of R_3: Phosphorylated once-bound surface receptors (R_4) bind to insulin (I) and become phosphorylated twice-bound surface receptors (R_3) with rate k_2. This reaction is reversible with rate k_{-2}. At the same time, phosphorylated twice-bound surface receptors (R_3) pass through the cell membrane with rate $k_{4'}$ to become phosphorylated twice-bound intracellular receptors (R_6). This process is reversible with rate $k_{-4'}$. Therefore, the synthesis rate of R_3 is

$$\dot{R_3} = k_2 I R_4 - k_{-2} R_3 + k_{-4'} R_6 - k_{4'} R_3 - d R_3. \tag{3.2.3}$$

The synthesis of R_4: In addition to the exchanges with R_1, R_2, and R_3, described above, phosphorylated once-bound surface receptors (R_4) pass though the membrane with rate $k_{4'}$, becoming phosphorylated once-bound intracellular receptors (R_7). That process is reversible with rate $k_{-4'}$. Therefore, the synthesis rate of R_4 is

$$\dot{R_4} = -k_2 I R_4 - k_{-3} P R_4 + k_3 R_2 + k_{-2} R_3 + k_{-4'} R_7 - k_{4'} R_4 - d R_4. \tag{3.2.4}$$

The synthesis rate of R_5: The source terms are the basal transcription to unbound unphosphorylated intracelluar receptors (R_5), b_6 and the positive feedback from the activated dFOXO, $l = \frac{f d \alpha F}{1+\alpha F}$, which is modeled by the Michaelis-Menten equation (α is a constant representing the affinity of activated dFOXO bound with the DNA strand. The stronger the affinity is, the larger the value of α will be). The phosphorylated twice-bound intracellular receptors (R_6) and phosphorylated once-bound intracellular receptors (R_7) are dephosphorylated and become unbound unphosphorylated

intracelluar receptors (R_5). Thus, the equation for the synthesis rate of R_5 is

$$\dot{R_5} = b_5 + l - dR_5 + k_5P(R_6 + R_7) + k_4R_1 - k_{-4}R_5 \tag{3.2.5}$$

The synthesis rate of R_6 and R_7: Through the interactions with free insulin receptors in cytoplasma (R_5) and bound insulin receptors in the cell membrane, we have

$$\dot{R_6} = k_{4'}R_3 - k_{-4'}R_6 - k_5PR_6 - dR_6 \tag{3.2.6}$$

$$\dot{R_7} = k_{4'}R_6 - k_{-4'}R_7 - k_5PR_7 - dR_7 \tag{3.2.7}$$

3.2.2 Chico/PI3K subsystem

In the insulin-like signaling pathway of *Drosophila melanogaster*, phosphorylated bound insulin receptors could phosphorylate chico, hence forming a chico-PI3K complex in the cell.

The synthesis rate of C_1: At the cell membrane the phosphorylated surface receptors (R_3 and R_4) phosphorylate Chico, according to a mass-action law with rate k_7. Also, phosphorylated Chico (C_2) is dephosphorylated by PTPases, according to a mass-action reaction with rate k_{-7}. Meanwhile, unphosphorylated Chico is translated from RNA with the rate denoted by b_c and degrades with the rate denoted by d_c. Therefore, the synthesis rate of unphosphorylated Chico is

$$\dot{C_1} = b_c - d_cC_1 + k_{-7}PC_2 - k_7C_1(R_3 + R_4) \tag{3.2.8}$$

The synthesis rate of C_2: Besides the interations with unphosphorylated Chico, the phosphorylated Chico (C_2) bind with deactivated PI3K (Φ_3) forming Chico-PI3K complex (Ξ) with the rate

of k_8. Therefore, the equation to describe the synthesis rate of phosphorylated Chico (C_2) is

$$\dot{C_2} = k_7 C_1(R_3 + R_4) - k_{-7} P C_2 + k_{-8}\Xi - k_8 \Phi_3 C_2 - d_c C_2. \tag{3.2.9}$$

The synthesis rate of Φ_3: Unphosphorylated PI3K (Φ_3) is translated form RNA with the rate denoted by b_p. The degradation rate of unphosphorylated PI3K (Φ_3) is denoted by d_p. Thus, the equation to describe the synthesis rate of unphosphorylated PI3K (Φ_3) is

$$\dot{\Phi_3} = b_p - d_p \Phi_3 + k_{-8}\Xi - k_8 \Phi_3 C_2 \tag{3.2.10}$$

The synthesis rate of Ξ: As mentioned above, through a mass-action reaction the production rate of the phosphorylated Chico-PI3K complex is denoted by k_8 and the dissociation rate is denoted by k_{-8}. With the degradation rate of phosphorylated PI3K-Chico complex to be d_{pc}, the synthesis rate of phosphorylated Chico-PI3K complex (Ξ) is

$$\dot{\Xi} = k_8 C_2 \Phi_3 - k_{-8}\Xi - d_{pc}\Xi. \tag{3.2.11}$$

3.2.3 Lipids subsystem

Adjacent to the cell membrane, the phosphorylated Chico-PI3K complex (Ξ) converts the substrate phosphatidylinositol 4,5-bisphosphate ($PI(4,5)P_2$) to the substrate product phosphatidylinositol 3,4,5-trisphosphate ($PI(3,4,5)P_3$). Furthermore, there is spontaneous phosphorylation and dephosphorylation causing transitions between these two states and between $PI(3,4,5)P_3$) and another, $PI(3,4)P_2$. Some of these are catalyzed by PTEN and SHIP, whose concentrations we take to be constant and are implicitly included in the rate constants shown below. We assume that the total amount of PIP is

conserved.

Let $L \equiv P_3 + P_4 + P_5$ be the total amount of PIP, the equations to describe the synthesis rates of P_3, P_4 and P_5 are

$$\dot{P_3} = k_{9p}\Xi P_5 + k_{9b}P_5 + k_{10}P_4 - k_{-9}P_3 - k_{-10}P_3, \tag{3.2.12}$$

$$\dot{P_4} = k_{-10}P_3 - k_{10}P_4, \tag{3.2.13}$$

$$\dot{P_5} = k_{-9}P_3 - (k_{9p}\Xi + k_{9b})P_5. \tag{3.2.14}$$

3.2.4 Akt subsystem

The synthesis rate of A and A_p: The lipid $PI(3,4,5)P_3$ (P_3) phosphorylates deactivated Akt at a rate proportional to the concentrations of the lipid and A with the rate constant denoted by k_{11}. Activated Akt is dephosphorylated spontaneously and becomes deactivated Akt with the rate k_{-11}. At the same time, deactivated and activated Akt (A and A_p) degrade at the rate of d_A. The deactivated Akt is translated from RNA with the rate of b_A. Hence, the equations to describe the synthesis rate of A and A_p are

$$\dot{A} = b_A - d_A A + k_{-11}A_p - k_{11}P_3 A \tag{3.2.15}$$

$$\dot{A_p} = k_{11}P_3 A - k_{-11}A_p - d_A A_p \tag{3.2.16}$$

3.2.5 dFOXO subsystem

In the dFOXO subsystem, different from previous subsystem, activated dFOXO (F) is unphosphorylated dFOXO and deactivated dFOXO (f) is phosphorylated dFOXO. The activated Akt phosphorylates the activated dFOXO, turning it from activated state to deactivated state. On the other hand, the deactivated dFOXO simultaneously unphophorylates itself back to activated state.

To model the process of Akt phosphorylating dFOXO, we notice that when activated Akt interacts with activated dFOXO, a small amount of temporary complex $[AF]$ forms quickly. Then $[AF]$ degrades to free activated Akt and phosphorylated dFOXO f.

Using the Michaelis-Menten formalism, assuming quasi steady state for this fast reaction, and ignoring higher order terms of small quantities, we find the production of phosphorylated dFOXO f is proportional to the amount of [AF]:

$$k_{12}\frac{\beta A_p F}{(\beta+1)F + A_p},$$

where β is the ratio of the rate at which the $[AF]$ forms to the rate at which it dissociates.

With the degradation rate of F and f being d_f and the basal transcriptional rate to F being b_F, we have

$$\dot{F} = -k_{12}\frac{\beta A_p F}{(\beta+1)F + A_p} + k_{-12}f + b_F - d_f F \tag{3.2.17}$$

$$\dot{f} = k_{12}\frac{\beta A_p F}{(\beta+1)F + A_p} - k_{-12}f - d_f f \tag{3.2.18}$$

The reaction process that dFOXO is phosphorylated by Akt is modelled as a MichaelisMenten kinetics. Specifically, let E be the free enzyme, S be the substrate, $[ES]$ be the enzyme-substrate complex, and E_t be the total enzyme (free enzyme plus enzyme-substrate complex). One have the following equation:

$$[\dot{ES}] = \frac{k_{on}ES}{E + [ES]} - k_{off}[ES].$$

At equilibrium point, $[\dot{ES}] = 0$. Therefore,

$$k_{on}ES = k_{off}[ES]E + k_{off}[ES]^2;$$

$$E = \frac{k_{off}[ES]^2}{k_{on}S - k_{off}[ES]}.$$

Let

$$\alpha = \frac{k_{on}}{k_{off}}.$$

Since the E_t is a constant, $E_t = E + [ES]$ gives us:

$$[ES] = \frac{\alpha E_t S}{\alpha S + E_t}.$$

Hence, the production rate of S' is:

$$q\frac{\alpha E_t S}{\alpha S + E_t}.$$

The activity of PTPases is modelled by an exponential function of activated Akt (A_p) ([17]).

$$P = exp(-kA_p) \tag{3.2.19}$$

3.3 Steady state of the system

The model consists of an eighteen ordinary differential equations with the concentration of the insulin as the model input. To analyse the relations of the components in the IIS pathway with the model input, the concentration of the insulin, I turn to look at the steady state of the ODE system. Thus, I need to solve the eighteen-equation algebraic system. The strategy to solve the algebraic system is by constructing an iteration mapping which converges to the solution of the algebraic system. Specifically, I separate the algebraic system into five subsystems as how the model is established in the above section. In the dFOXO subsystem, I solve the activated dFOXO as a function of the activated Akt.

$$F = \frac{-(k_{12}\beta + k_{-12} + d_F)A_p - (b_F + k_{-12}\frac{b_F}{d_F})(\beta+1)}{2(d_F + k_{-12})(\beta+1)} + \frac{\sqrt{((k_{12}\beta + k_{-12} + d_F)A_p - (b_F + k_{-12}\frac{b_F}{d_F})(\beta+1))^2 + 4(d_F + k_{-12})(\beta+1))((b_F + k_{-12}\frac{b_F}{d_F})A_p))}}{2(d_F + k_{-12})(\beta+1)} \tag{3.3.1}$$

and

$$P = exp(-0.003A_p).$$

In the Akt subsystem, I solve the activated Akt as a function of the $PI(3,4,5)P_3$.

$$A_p = \frac{a_A k_{11} P_3}{k_{11}P_3 + k_{-11} + d_A}.$$

In the lipid subsystem, I solve the $PI(3,4,5)P_3$ as a function of the phosphorylated Chico-Pi3k complex.

$$P_3 = \frac{1}{1 + 29/31 + \frac{k_{-9}}{k_{-9p}\Xi + k_{9b}}}.$$

In the Chico subsystem, I solve the phosphorylated Chico-Pi3k complex as a function of the insulin-bounded receptors on the cell membrane.

$$\Xi = \frac{-B - \sqrt{B^2 - 4AC}}{2A}$$

where

$$A = \frac{k_8(d_c + k_7(R_3 + R_4))}{k_{-7}P + d_c + k_7(R_3 + R_4)};$$

$$B = \frac{-k_8(d_c + k_7(R_3 + R_4))(a_p + a_c - \frac{b_c}{d_c + k_7(R_3 + R_4)}}{k_{-7}P + d_c + k_7(R_3 + R_4)} - d - k_8;$$

$$C = \frac{k_8(d_c + k_7(R_3 + R_4))(a_p + a_c - \frac{b_c}{d_c + k_7(R_3 + R_4)}}{k_{-7}P + d_c + k_7(R_3 + R_4)}.$$

For the insulin receptor subsystem, I solve the insulin-bounded receptors on the cell membrane as a function of the activated dFOXO. Then I compose those functions together to get an iteration of the activated dFOXO. Finally, I keep iterating the composition function until the iteration converges.

In the steady state, the total amount of insulin receptor is equal to:

$$R_1 + R_2 + R_3 + R_4 + R_5 + R_6 + R_7 = \frac{b_5 + l}{d}.$$

Assuming the degradation rate of Chico, phosphorylated Chico and Chico-PI3K complex are the same, i.e. $d_c = d_p = d_{pc}$, one can derive that the total amount of Chico is equal to:

$$C_1 + C_2 + \Xi = \frac{b_c}{d_c}$$

and

$$\Phi + \Xi = \frac{b_p}{d_p}.$$

Similarly, in the Akt subsystem, one can derive that the total amount of Akt is equal to:

$$A + A_p = \frac{b_a}{d_a},$$

and in the dFOXO subsystem, the total amount of dFOXO is equal to:

$$F + f = \frac{b_F}{d_f}.$$

I define that

$$a_5 = \frac{b_5}{d},$$

$$feedback = \frac{fb}{d},$$

$$a_c = \frac{b_c}{d_c},$$

$$a_p = \frac{b_p}{d_p},$$

$$a_A = \frac{b_a}{d_a}$$

and

$$a_F = \frac{b_F}{d_f}.$$

Those variables serve as the parameters regulating the total amount of insulin receptors, Chico, PI3k, Akt and dFOXO. In *Drosophila melanogaster*, the concentrations of those proteins are different in various organs. Thus, by introducing those parameters, I could investigate the allometries of various organs by manipulating the values of those parameters. For any fixed set of parameters a_5, a_c, a_p, a_A, a_F, $feedback$ and model input, the concentration of insulin I, I compute the concentration of activated dFOXO, F. Hence, varying the concentration of insulin I, I get a curve of the concentration of activated dFOXO F. For instance, let $a_5 = 1pM$, $a_c = 1pM$, $a_p = 0.1pM$, $a_A = 5pM$, $a_F = 5pM$, $feedback = 0.5pM$, I has the curve in figure 3.2.

The dFOXO is a negative growth factor. In order to establish the relation between the concentration of the insulin and the organ size of flies, I used empirical data to estimate the relationship between dFOXO activity and organ size, and hence the nutritional plasticity of organ size. We plot the relationship between wing Size and active dFOXO. The size of the wing decreases as the concentration of active dFOXO increases. Moreover, there is a lower limit for the wing size. The size of the wing is never smaller than 8×10^5 no matter what the concentration of active dFOXO and environmental conditions are. Thus, the natural way to fit the relationship between the wing size and the concentration of active FOXO is to use the rational function.

$$Organsize = \frac{a}{F + b} + c,$$

where F represents the concentration of activated dFOXO, from the empirical data of wing cell number of flies. I observe from the empirical data that the lower limit for the wing size, c, is 8×10^5. Then we use the Least Square method to fit the parameter a and b. Since the relationship of Wing size and active dFOXO differs as the environmental conditions vary, the coefficient a and b also vary. From our methods, parameter a ranges from 2.5×10^5 to 3.5×10^5 and b ranges from

0.4 to 0.6. To simplify the computation and analysis, I pick a to be 3×10^5 and b to be 0.5. Hence, fixing the same parameters as $a_5 = 1pM$, $a_c = 1pM$, $a_p = 0.1pM$, $a_A = 5pM$, $a_F = 5pM$, $feedback = 0.5pM$, the relation between the number of cells of wing and the concentration of insulin is shown in figure 3.3.

3.4 The nutritional plasticity

In *Drosophila melanogaster*, the response of the body and organ size to changes in developmental nutrition is called the nutritional plasticity. Malnutrition during development reduces adult body size of *Drosophila melanogaster*. However, not all the organs respond to the malnutrition to the same extent. Some organs, for example, the male genitalia, are remarkably resistant to changes in developmental nutrition. Like the mammalian brain, they are more or less the same size in large and small individuals. One hypothesis is that the nutritional plasticity is regulated through the IIS pathway. The amounts of gene expressions of components in the IIS pathway are the factor affecting the nutritional plasticity in Drosophila. Hence, I establish a mathematical model to represent the nutritional plasticity. The nutritional plasticity in the paper is defined to be the difference of the logarithmic organ size at two insulin concentration levels. Specifically, let $OrganSize = S(I)$ be the function of the organ size with respect to the concentration of insulin. I define:

$$Plasticity = log(S(I + \delta)) - logS((I)) \tag{3.4.1}$$

where $I + \delta$ and I are two different levels of insulin concentration. Without further remark, I take $I = 20pM$ and $\delta = 1000pM$ in this dissertation.

3.5 The results

In figure 3.4, the nutritional plasticity is regulated by the total gene expression of insulin receptors. Fixing the gene expression of Chico, PI3K, Akt and dFOXO to be $1pM$, $0.1pM$, $5pM$ and $5pM$ respectively, the nutritional plasticity increases as the gene expression of total insulin receptors increase. But the rate of increase (the tangent line of the curve) decreases.

In figure 3.5, the nutritional plasticity is regulated by the total gene expression of Chico. Fixing the gene expression of Inr, PI3K, Akt and dFOXO to be $5pM$, $0.1pM$, $5pM$ and $5pM$ respectively, the nutritional plasticity increases then decreases as the gene expression of total insulin receptors increase.

In figure 3.6, the nutritional plasticity is regulated by the total gene expression of PI3K. Fixing the gene expression of Inr, Chico, Akt and dFOXO to be $5pM$, $1pM$, $5pM$ and $5pM$ respectively, the nutritional plasticity increases then decreases as the gene expression of total insulin receptors increase.

In figure 3.7, the nutritional plasticity is regulated by the total gene expression of Akt. Fixing the gene expression of Inr, Chico, PI3K and dFOXO to be $5pM$, $1pM$, $0.1pM$ and $5pM$ respectively, the nutritional plasticity increases then decreases as the gene expression of total insulin receptors increase.

In figure 3.8, the nutritional plasticity is regulated by the total gene expression of dFOXO. Fixing the gene expression of Inr, Chico, PI3K and Akt to be $5pM$, $1pM$, $0.1pM$ and $5pM$ respectively, the nutritional plasticity increases then decreases as the gene expression of total insulin receptors increase. There is a non-linear relationship between FOXO expression and nutritional plasticity. This graph is coincident with the real experiment results (See figure 3.9). ([15])

From the simulation of the figure 3.8, the nutritional plasticity has a nonlinear relationship

with the total gene expression of dFOXO. For those organs with either very high or very low total gene expression of dFOXO, they are more or less insensitive to the change of nutrition. The high nutritional plasticity is achieved when total gene expression of dFOXO is at medium level. This does not change when the total gene expression of insulin receptosr increase. However, maximum nutritional plasticity increases as the total gene expression of insulin receptors increase. In addition, the value of total gene expression of dFOXO at which the maximum is achieved increases as well. See the figure 3.10 for a three dimensional graph of the nutritional plasicity versus the total gene expression of insulin receptors and the total gene expression of dFOXO when the gene expression of Chico, PI3K and Akt to be $1pM$, $0.1pM$ and $5pM$ respectively.

In the three dimensional figure 3.11 of the nutritional plasticity versus the gene expression of Akt and dFOXO, the ridge is in the direction of Akt. That is due to the bell curve of the nutritional plasticity versus the dFOXO.

3.6 Model coefficients

Here lists those model coefficients that are taken from [11]:

$k_1 = 6 \times 10^{-5} pM^{-1} \cdot min^{-1}$;

$k_{-1} = 0.2 min^{-1}$;

$k_2 = k_1 min^{-1}$;

$k_{-2} = 20 min^{-1}$;

$k_3 = 2500 min^{-1}$;

$k_{-3} = 0.2 min^{-1}$;

$k_4 = 0.0003 min^{-1}$;

$k_{-4} = 0.003 min^{-1}$;

$k_{4'} = 2.1 \times 10^{-3} min^{-1}$;

$k_{-4'} = 2.1 \times 10^{-4} min^{-1}$;

$k_6 = 0.461 min^{-1}$;

$k_7 = 4.638 min^{-1}$;

$k_{-7} = 1.396 min^{-1}$;

$k_8 = 0.707 pM^{-1} \cdot min^{-1}$;

$k_{-8} = 10 min^{-1}$;

$k_{-9} = 42.148 min^{-1}$;

$k_{9b} = 0.131 min^{-1}$;

$k_{9p} = 1.390 min^{-1}$;

$k_{10} = 2.961 min^{-1}$;

$k_{-10} = 2.77 min^{-1}$;

$k_{11} = 2.484 min^{-1}$;

$k_{-11} = 6.932 min^{-1}$.

The new coefficients of the ordinary differential equations are:

$k = 0.03$;

$k_{12} = 30 pM^{-1} \cdot min^{-1}$;

$k_{-12} = 1 min^{-1}$;

$\alpha = 1$;

$\beta = 2$;

$d_5 = 0.01 min^{-1}$;

$d_c = 0.01 min^{-1}$;

$d_p = 0.01 min^{-1}$;

$d_{pc} = 0.01 min^{-1}$;

$d_A = 0.01 min^{-1}$;

$d_f = 0.01 min^{-1}$;

$b_5 : 0.1 - -10 pM \cdot min^{-1}$;

$b_c : 0.1 - -10 pM \cdot min^{-1}$;

$b_p : 0.1 - -10 pM \cdot min^{-1}$;

$b_a : 0.1 - -10 pM \cdot min^{-1}$;

$b_F : 0.1 - -10 pM \cdot min^{-1}$.

The illustration of the abbreviations in the model are:

ILP:

Insulin (protein) is a hormone central to regulating carbohydrate and fat metabolism in the body. It is the model input which binds to inr and initiates a signal transduction cascade involving the phosphorylation of multiple intermediate proteins.

Inr:

It is a protein kinase on the cell membrane which can bind with insulin. When insulin binds to the insulin receptor on the cell surface, the receptor changes shape so that the kinase regions inside the cell become activated. The activated insulin receptor then activates a number of different targets within the cell.

Chico/IRS:

Insulin receptor substrate is a protein containing a phosphotyrosine binding-domain (PTB-domain). The insulin receptor contains a NPXpY domain. The PTB-domain binds with the NPXpY domain. Thus, IRS binds with insulin receptor.

PI3K:

Phosphatidylinositol 3-kinases or PI 3-kinases are a family of enzymes involved in cellular functions such as cell growth, proliferation, differentiation, motility, survival and intracellular traffick-

ing. They interact with IRS (insulin receptor substrate) through a series of phosphorylation events.

PI(3,4)P2, PI(4,5)P2, PI(3,4,5)P3:

Various phosphoinositol lipids on the cell membrane.

Akt:

Akt, also known as Protein Kinase B (PKB), is a serine/threonine protein kinase. Akt possesses a protein domain known as a PH domain (Pleckstrin Homology domain). This domain binds to PIP3 on the cell membrane. Once Akt is correctly positioned at the membrane via binding of PIP3, it can then be phosphorylated and become activated.

FOXO:

FOXO is a transcription factor which can negatively regulate the body growth. FOXO can be phosphorylated by activated Akt at three conserved residues. Phosphorylated FOXO exports from the nucleus to the cytoplasm, thereby inhibiting FOXO-dependent transcription.

PTP:

PTPases are a class of enzymes that can regulate tyrosine kinase activity by removing a phosphate.

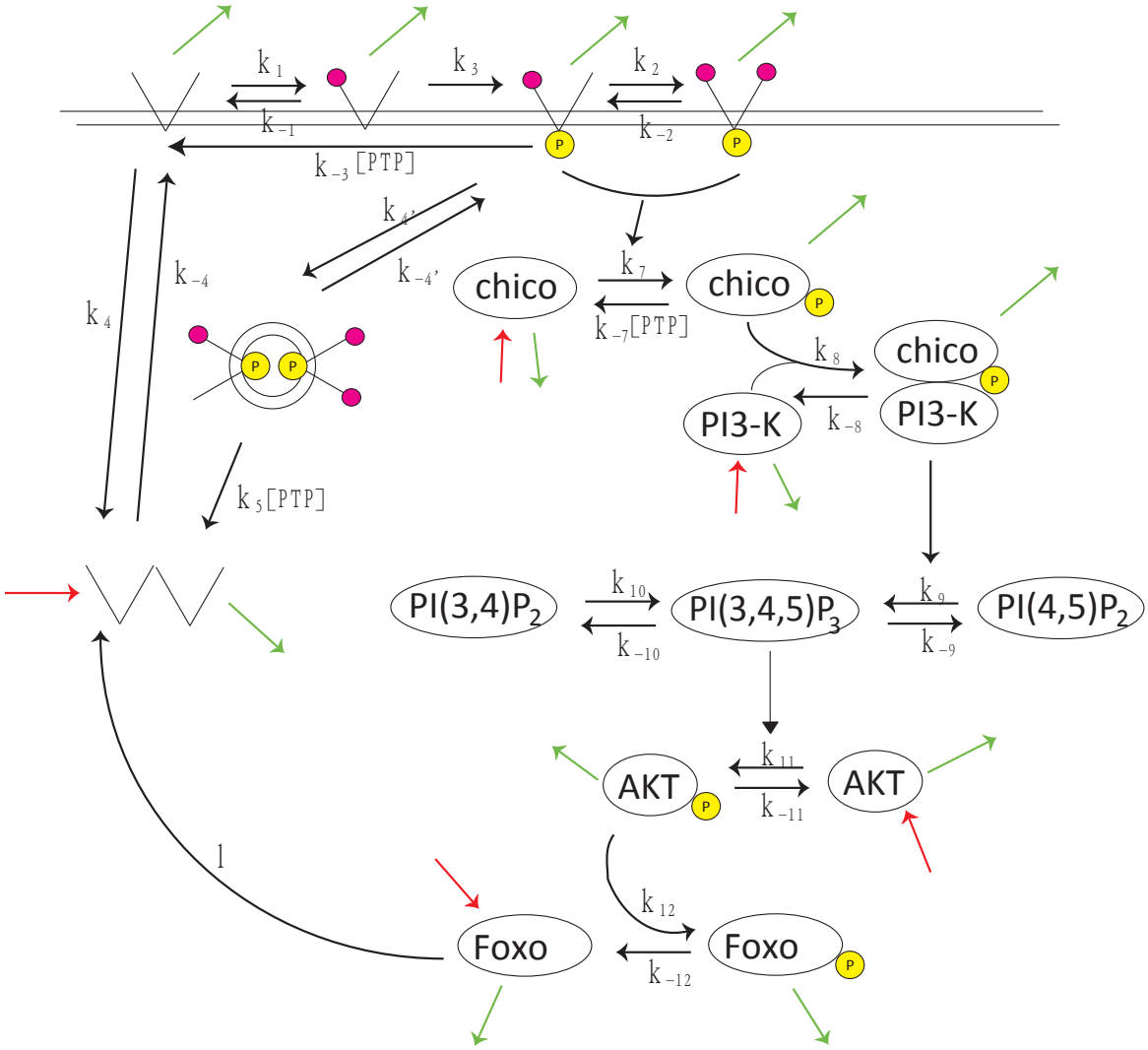

Figure 3.1: The structure of IIS pathway.

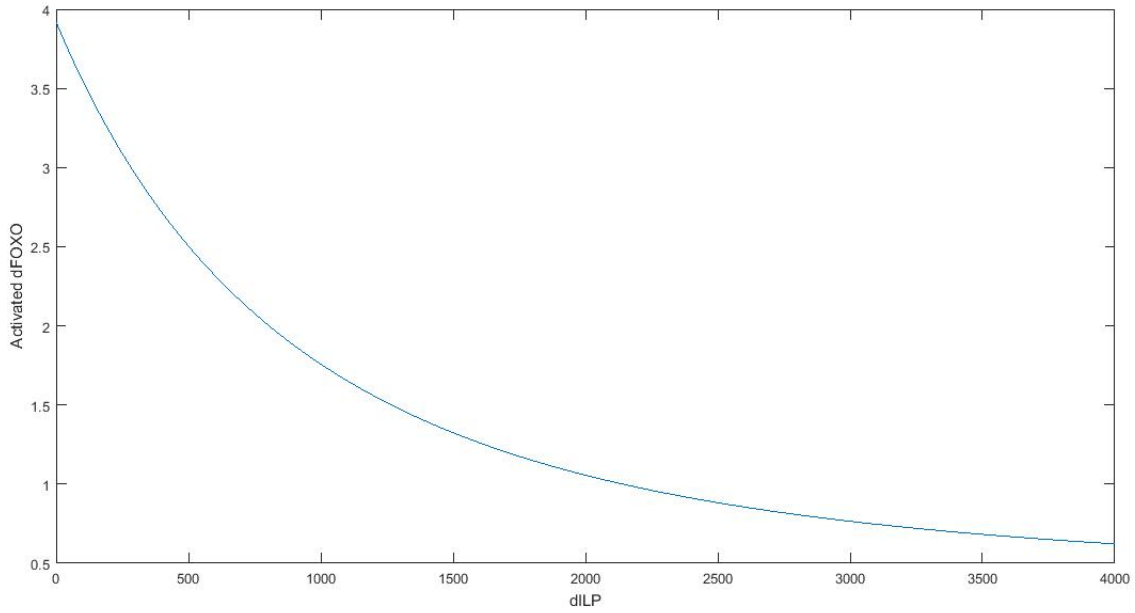

Figure 3.2: The concentration of activated dFOXO v.s. the concentration of insulin.

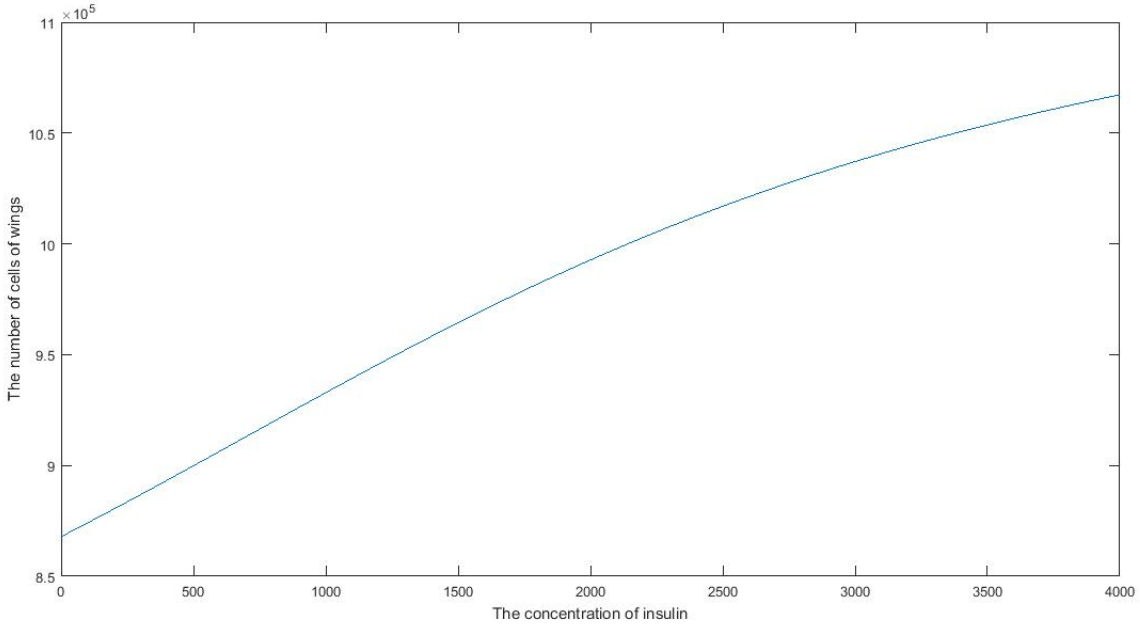

Figure 3.3: The number of cells of wing v.s. the concentration of insulin.

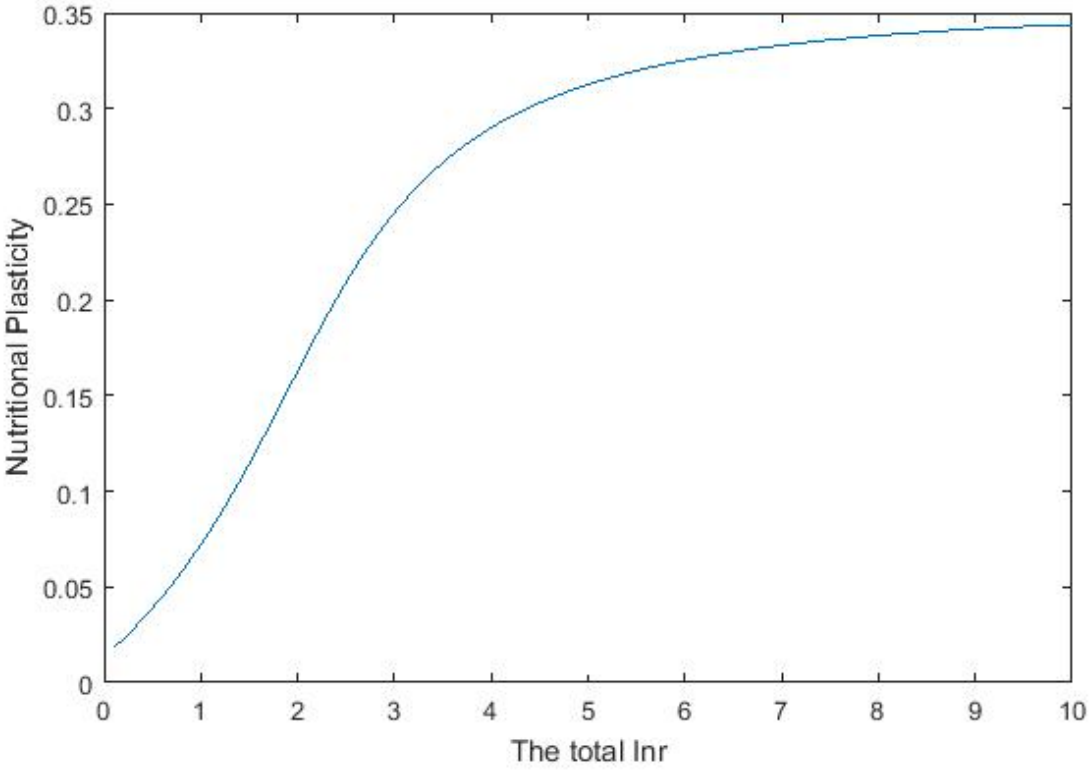

Figure 3.4: The nutritional plasticity v.s. the gene expression of Inr.

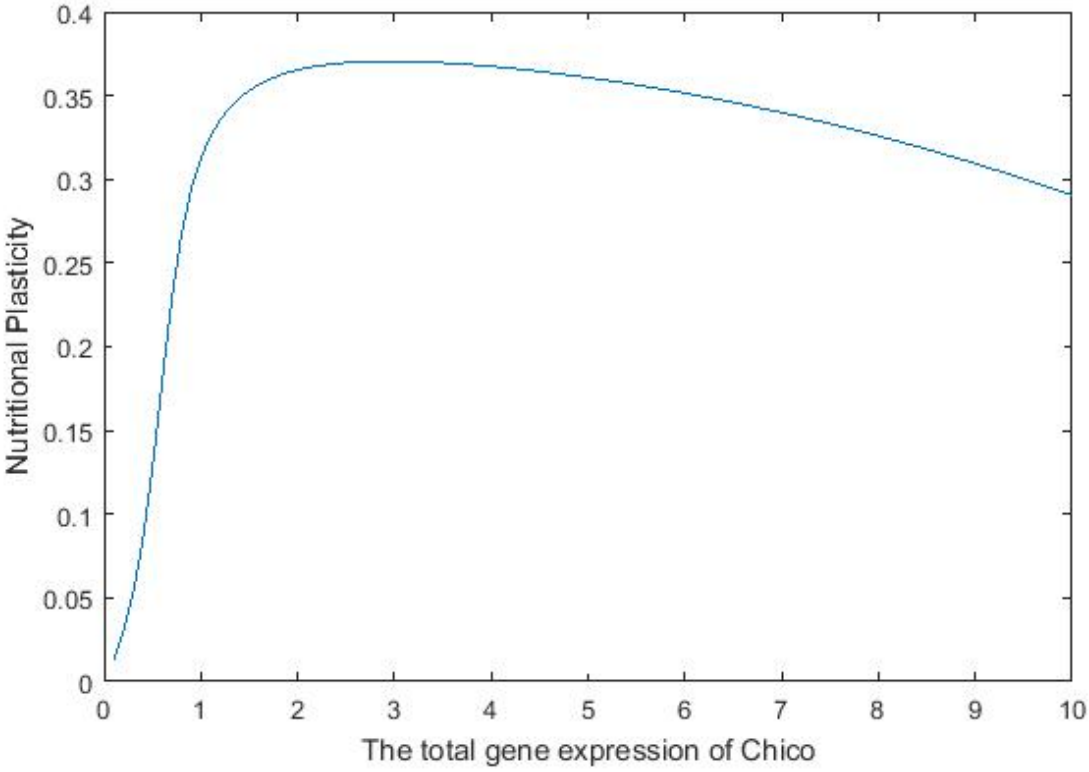

Figure 3.5: The nutritional plasticity v.s. the gene expression of Chico.

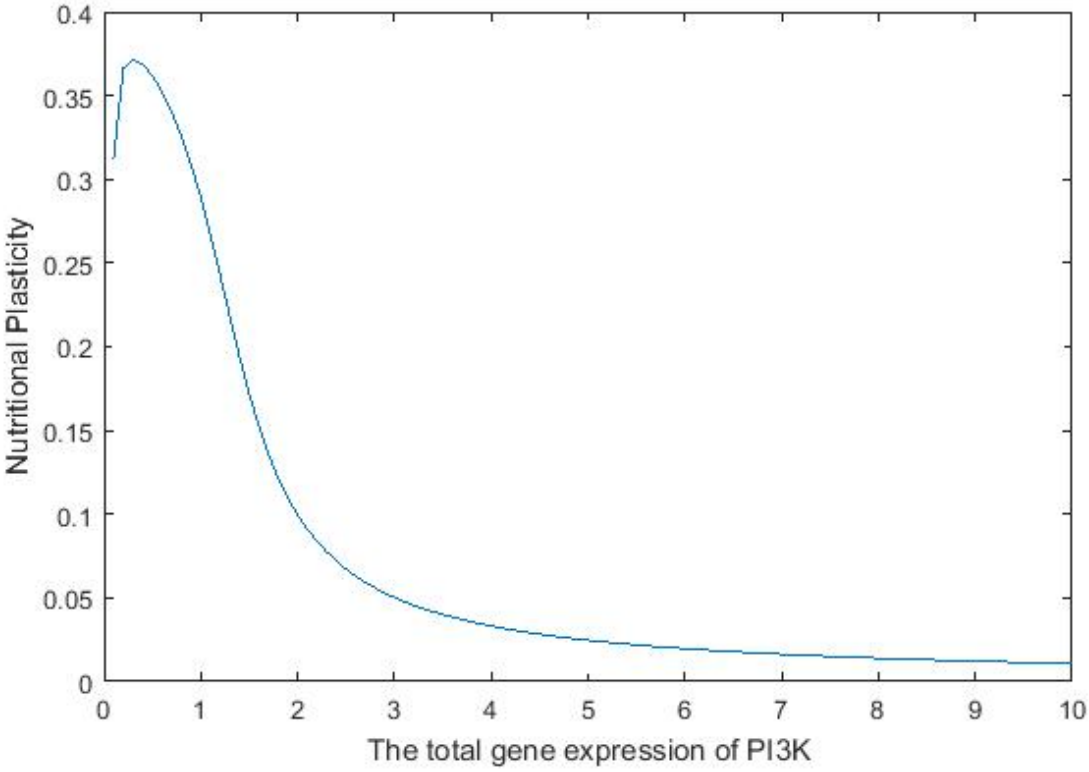

Figure 3.6: The nutritional plasticity v.s. the gene expression of PI3K.

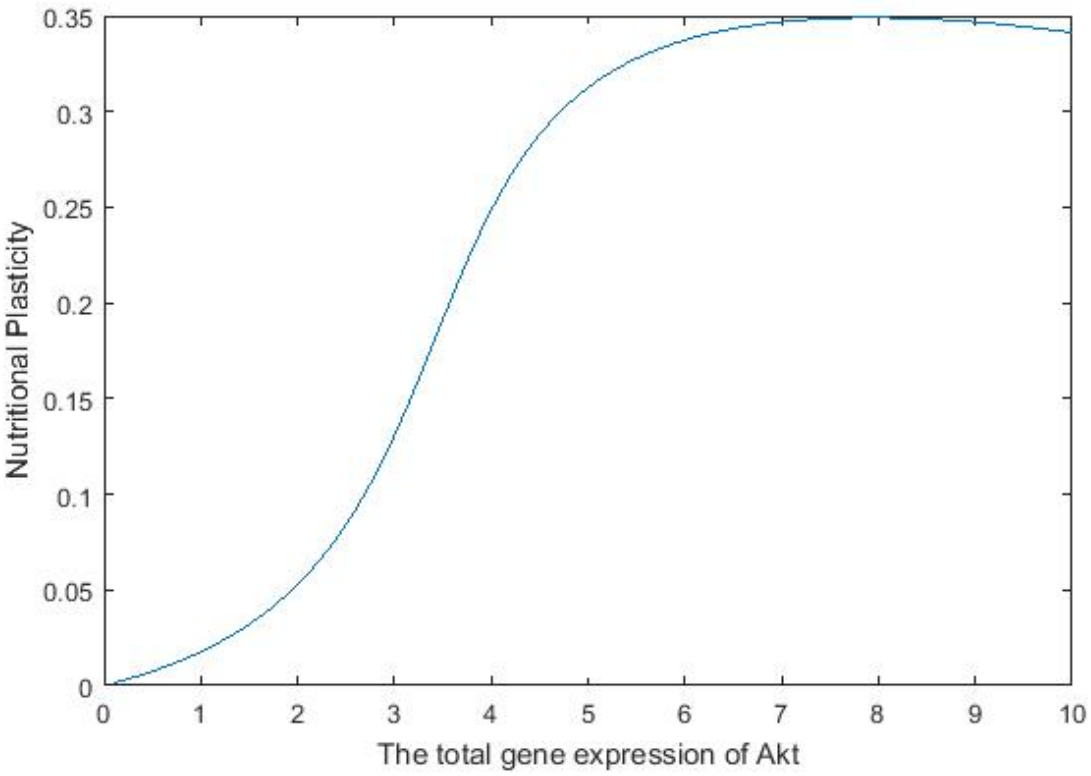

Figure 3.7: The nutritional plasticity v.s. the gene expression of Akt.

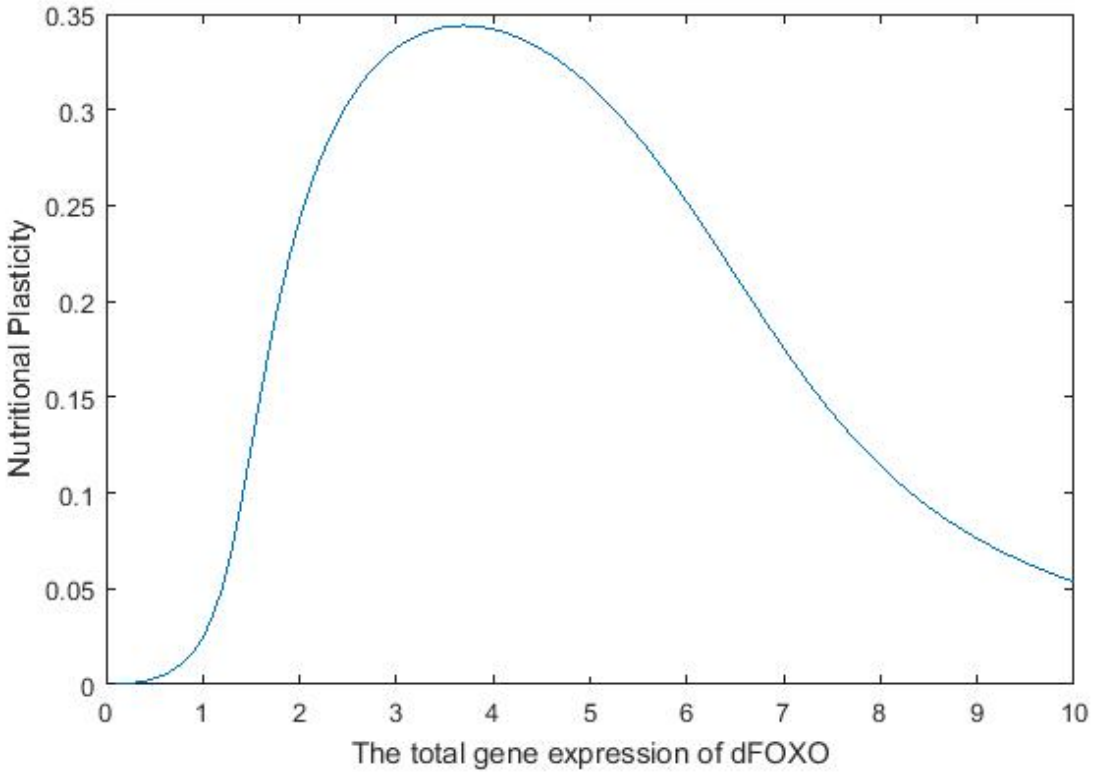

Figure 3.8: The nutritional plasticity v.s. the gene expression of dFOXO.

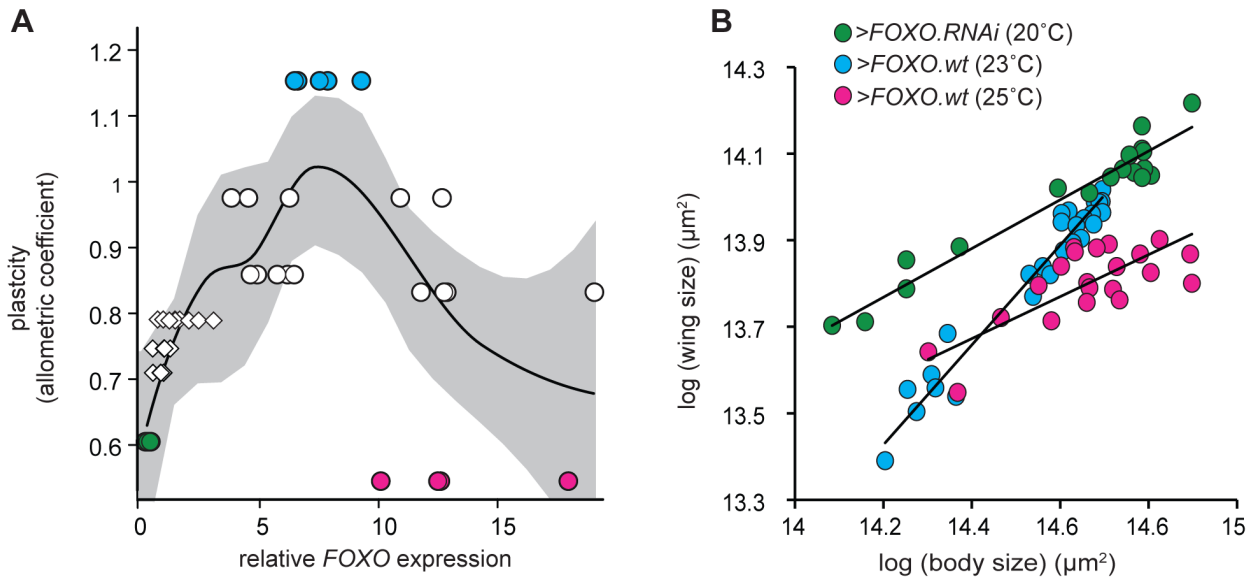

Figure 3.9: There is a non-linear relationship between dFOXO expression and nutritional plasticity
.

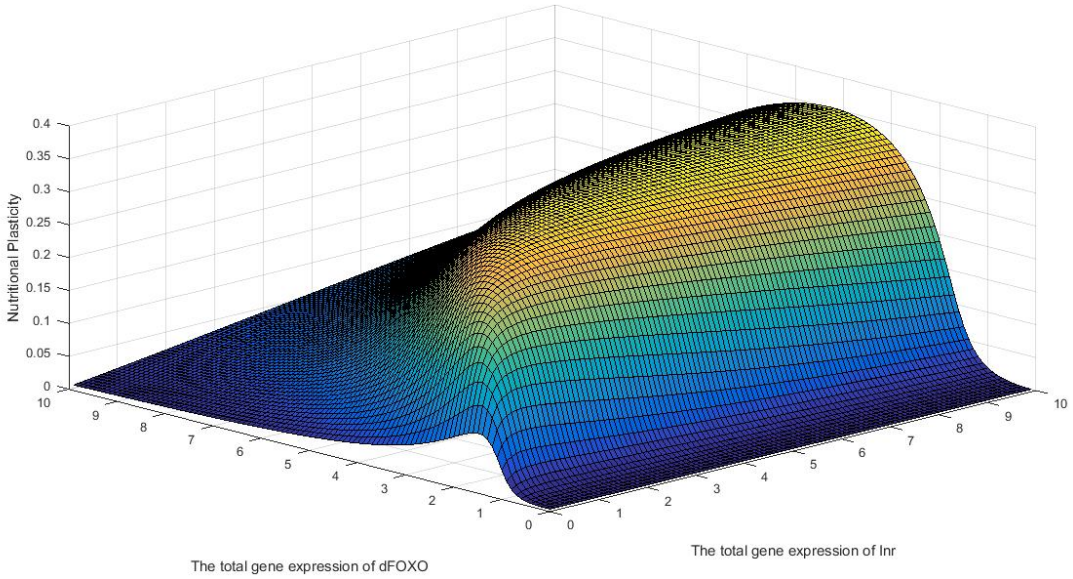

Figure 3.10: The nutritional plasticity v.s the gene expression of Inr and dFOXO.

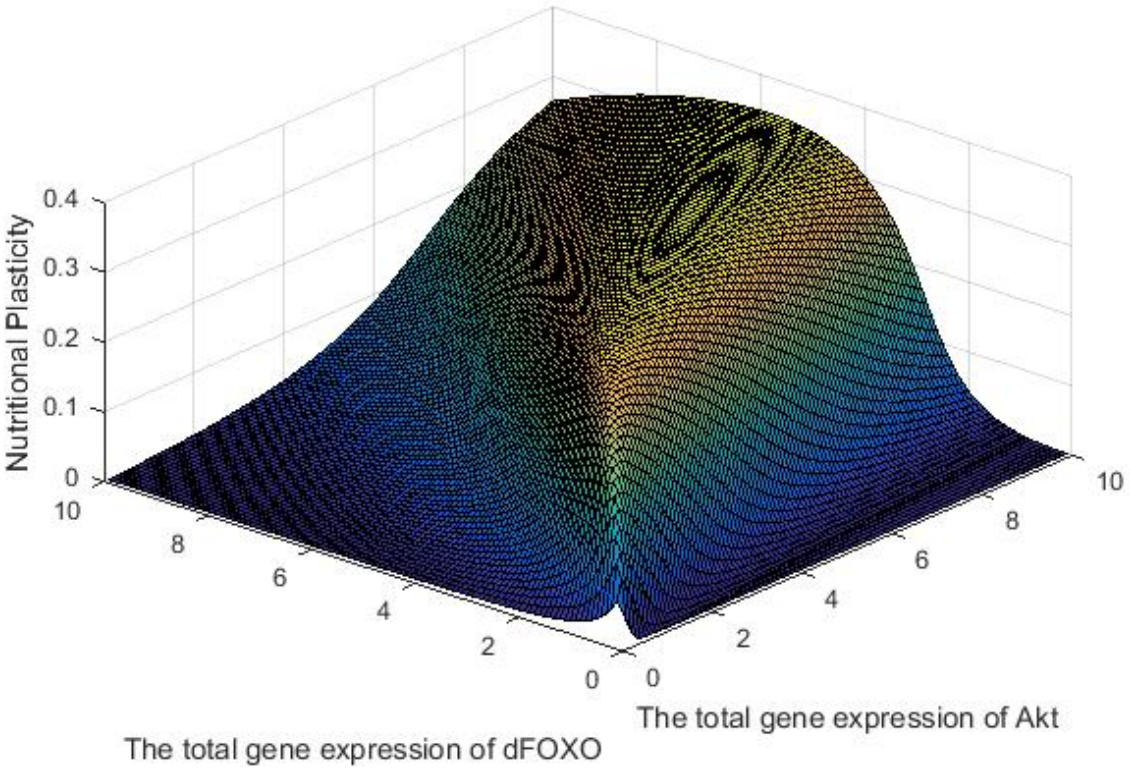

Figure 3.11: The nutritional plasticity v.s the gene expression of Akt and dFOXO.

Chapter 4

A PDE model

4.1 Preliminary

The insulin and insulin-like signaling (IIS) pathway propagates a signal from receptors in the cell membrane to the nucleus via numerous molecules. Some of these molecules reside on or contiguous to the cell membrane, some reside in or contiguous to the nucleus and some are in the cytosol, being transported between these two regions in a somewhat stochastic way. Included in this pathway is the forkhead transcription factor FOXO, which promotes the expression of negative growth regulators ([12]). FOXO is negatively regulated by the insulin signaling pathway, and it is the reduction in insulin signaling and the resulting activation of FOXO that is, in part, responsible for inhibiting organ growth in conditions of reduced nutrition ([4]). The result is that organ growth is nutritionally plastic. However, different organs show different levels of nutritional plasticity, essential to ensuring that certain key organs, for example the mammalian brain, are largely spared the effects of malnutrition. Recent research has suggested that these differences in nutritional plasticity are mediated by differences in the structure of the insulin-signaling pathway in different organs. However, how changes in the structure of the insulin signaling pathway affects how the pathway regulates growth with respect to nutrition is unclear. Here we use mathematical modeling to help solve this problem.

In the ODE model, the variables of the equations are the circulating concentration of each components of IIS pathway. We don't model the movement of the molecular of proteins components

of IIS. However, although many of the protein components of the insulin signaling pathway are attached to, or associated with, the cell membrane they are all at some point transported through the cytoplasm. All proteins are synthesized at the endoplasmic reticulum (ER), which is contiguous with the nuclear membrane. The proteins are then packaged into vesicles, first by the ER and then by the Golgi apparatus, before these vesicle, and the proteins within them, are transported to their final destination. Vesicle transport is through the action of molecular motors, e.g. kinesin, which attach to the vesicle and walk it along the microtubules that form the cytoskeleton of the cell. Because the transportation process has a stochastic aspect to it, due to the distribution of motors and micro- tubules (or other scaffolding) and the processivity of the motors, this is modeled as an enhanced or directional diffusive process. For simplicity we use a spherically symmetric cell with the nuclear shell having radius r_1 and the cell membrane having radius r_2 ($r_1 < r_2$).

Among other things, this diffusive transport builds a delay into the dynamics described in [11], which may be important in regulation. We also include degradation and basal transcription of molecules into the model. As mentioned above, the growth of organs is negativly regulated in part by the transcription factor FOXO, the active state of which resides in the nucleus. A protein kinase, Akt, downstream from the insulin receptors, in its active (phosphorylated) state, deactivates FOXO by phosphorylating it. Phosphorylation of FOXO by Akt both inhibits its activity as a transcription factor and causes it to be transported out of the nucleus. The inactive FOXO in the cytoplasm can be reactivated and targeted for nuclear localization through phosphorylation or monoubiquitination by proteins in other signaling pathways. Importantly, activated FOXO promotes the transcription of the insuin receptor, creating a negative feedback loop between the top and the bottom of the pathway ([7]). Thus, our system becomes more complex by adding both molecular species with transcriptional feedback, and spatial transport of some molecules. Part of our purpose for this is to determine the mechanism whereby organ size plasticity is regulated. We believe that this regulation

of plasticity is achieved through the insulin-signaling pathway in general and FOXO specifically. Our model explores that hypothesis.

4.2 The Partial Differential Equations model of the IIS pathway

We divide the system into several coupled subsystems, starting with the

4.2.1 Insulin receptors subsystem

Let I denote the concentration of insulin, which is a constant in this paper (we take two values of I when computing sensitivity). An insulin receptor in the cell membrane may bind one or two insulin molecules and when bound, autophosphorylation occurs and so initiates a signal transduction cascade. Receptors may also reside temporarily in the cytosol, where they are transported to the cell membrane.

Thus we have the state variables:

Receptors:

$R_1(t)$, concentration of unbound unphosphorylated cell-surface receptors,

$R_2(t)$, concentration of once-bound unphosphorylated cell-surface receptors,

$R_3(t)$, concentration of phosphorylated twice-bound cell-surface receptors,

$R_4(t)$, concentration of phosphorylated once-bound cell-surface receptors,

$R_5(r,t)$, concentration of unbound unphosphorylated intracellular receptors,

$R_6(r,t)$, concentration of phosphorylated twice-bound intracellular receptors,

$R_7(r,t)$, concentration of phosphorylated once-bound intracellular receptors.

PTP:

$P(r,t)$: A prefactor representing the relative activity of PTPases (the class of enzymes that regulate tyrosine kinase activity by removing a phosphate) in the cell. This factor depends upon the level of activated Akt, which varies according to a partial differential equation coupled to the rest of the system.

FOXO:

$F(r,t)$, concentration of activated FOXO,

$f(r,t)$, concentration of deactivated FOXO.

The synthesis of R_1: Free insulin receptors (R_1) on the membrane bind to insulin (I) and become once-bound unphosphorylated surface receptors (R_2) at the rate k_1. That reaction is reversible with rate k_{-1}. Phosphorylated once-bound surface receptors (R_4) are dephosphorylated by PTPases, release their insulin and become unbound unphosphorylated surface receptors (R_1) with rate $k_{-3}P$. At the same time, free surface receptors (R_1) pass through the cell membrane to become intracellular receptors (R_5) with rate k_4 and the intracellular receptors attach to the cell membrane, becoming surface receptors with rate k_{-4} ([8],[9]). Finally, a certain fraction (d) of receptors degrades and is lost. Therefore, the synthesis rate of free receptor on the membrane, R_1, is expressed by

$$\dot{R_1} = -k_1 I R_1 + k_{-1} R_2 + k_{-3} P R_4 + k_{-4} R_5(r_2, t) - k_4 R_1 - d R_1. \tag{4.2.1}$$

The synthesis of R_2: In addition to the exchanges with R_1, described above, the once-bound unphosphorylated surface receptors (R_2) degrade at the same rate d and are phosphorylated to become phosphorylated once-bound surface receptors (R_4) at the rate k_3. Therefore, the synthesis

rate of R_2 is

$$\dot{R_2} = k_1 I R_1 - k_{-1} R_2 - k_3 R_2 - d R_2. \tag{4.2.2}$$

The synthesis of R_3: Phosphorylated once-bound surface receptors (R_4) bind to insulin (I) and become phosphorylated twice-bound surface receptors (R_3) with rate k_2. This reaction is reversible with rate k_{-2}. At the same time, phosphorylated twice-bound surface receptors (R_3) pass through the cell membrane with rate $k_{4'}$ to become phosphorylated twice-bound intracellular receptors (R_6). This process is reversible with rate $k_{-4'}$. Therefore, the synthesis rate of R_3 is

$$\dot{R_3} = k_2 I R_4 - k_{-2} R_3 + k_{-4'} R_6(r_2, t) - k_{4'} R_3 - d R_3. \tag{4.2.3}$$

The synthesis of R_4: In addition to the exchanges with R_1, R_2, and R_3, described above, phosphorylated once-bound surface receptors (R_4) pass though the membrane with rate $k_{4'}$, becoming phosphorylated once-bound intracellular receptors (R_7). That process is reversible with rate $k_{-4'}$. Therefore, the synthesis rate of R_4 is

$$\dot{R_4} = -k_2 I R_4 - k_{-3} P R_4 + k_3 R_2 + k_{-2} R_3 + k_{-4'} R_7(r_2, t) - k_{4'} R_4 - d R_4. \tag{4.2.4}$$

The synthesis of R_5: The gene responsible for creating insulin receptors is transcribed in the nucleus and the resulting RNA passes through pores in the nuclear shell entering the cytoplasm. Once in the cytoplasm, with the help of a ribosome, translation starts to the protein (receptor) and is completed in the ER (endoplasmic reticulum), which is contiguous to the nucleus. The receptor is then packaged into vesicles (the vesicle membrane holds the receptor which is a transmembrane protein) and is taken to the Golgi apparatus, and then finally the cellular surface membrane. All via transport vesicles that are moved by one of the motor proteins along microtubules. Here, we

simplify this process by postulating the production of free insulin receptors (R_5) on the nuclear surface ($r = r_1$) due in part to the activated transcription factor FOXO which enhances basal transcription. The resulting receptors are actively transported to the outer cell membrance, but in a stochastic way. Thus, R_5 has a spatio-temporal distribution that is governed by an equation with advection and diffusion terms, as well as reaction terms, exchanging between other states, and a degradation term. The advection-diffusion operator we employ has the form

$$Lu \equiv D\Delta u - \delta\nabla \cdot (\frac{\mathbf{x}}{|\mathbf{x}|}u),$$

giving radially-directed transport towards the cell membrane. In the equations below, we express this operator in radial coordinates since we assume spherical symmetry. Boundary conditions represent a FOXO-dependent source at r_1 and a sink at r_2, as receptors leave the cytoplasm to become embedded in the cell membrane. The way in which activated FOXO (F) operates in creating free receptors at the nucleus is modeled using the Michaelis-Menten relation, giving a term $l = \frac{\gamma\alpha F}{1+\alpha F}$, where α is a constant representing the affinity of FOXO binding to DNA and γ is a rate factor. We may also consider a mass-action reaction rate, which gives qualitatively similar results. The exchanges between other states in the cytoplasm include only intracellular receptors which are phosphorylated and have one or two insulin molecules bound become unphosphorylated at a rate k_6P, releasing their insulin, thereby contributing to R_5.

Therefore, the distribution of R_5 is described by

$$\frac{\partial R_5}{\partial t} = \frac{D}{r^2}\frac{\partial}{\partial r}(r^2\frac{\partial R_5}{\partial r}) - \frac{\delta}{r^2}\frac{\partial}{\partial r}(r^2R_5) - dR_5 + k_5P(R_6 + R_7), \tag{4.2.5}$$

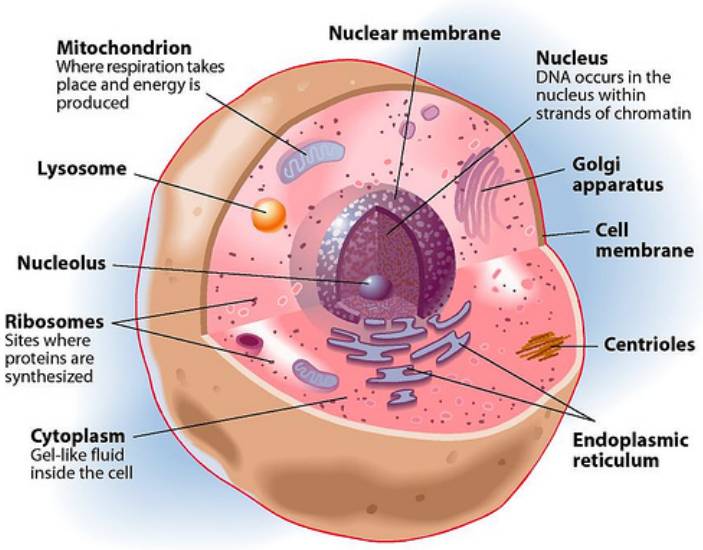

Figure 4.1: The structure of the cell.

with the boundary conditions obtained through a flux calculation,

$$D\frac{\partial R_5}{\partial r}(r_1,t) - \delta R_5(r_1,t) = -l - b_5, D\frac{\partial R_5}{\partial r}(r_2,t) - \delta R_5(r_2,t) = k_4 R_1 - k_{-4} R_5, \ t > 0.$$

The synthesis of R_6 and R_7: As described above, the twice-bound (R_6) and once-bound (R_7) intracellular receptors may pass through the membrane to become surface receptors, and vice-versa. Also these receptors become unphosphorylated at a rate k_6, releasing their insulin, and contributing to R_5. While in the cytosol, we assume that these receptors are actively transported towards the plasma membrane in the same way as the free receptos, that is, according to an advective and diffusive process. Again, their degradation rate is given by d. Therefore, the synthesis rates of R_6 and R_7 are

$$\frac{\partial R_6}{\partial t} = \frac{D}{r^2}\frac{\partial}{\partial r}(r^2\frac{\partial R_6}{\partial r}) - \frac{\delta}{r^2}\frac{\partial}{\partial r}(r^2 R_6) - dR_6 - k_5 P R_6, \tag{4.2.6}$$

with boundary conditions

$$D\frac{\partial R_6}{\partial r}(r_1,t) - \delta R_6(r_1,t) = 0, \quad D\frac{\partial R_6}{\partial r}(r_2,t) - \delta R_6(r_2,t) = k_4' R_3 - k_{-4}' R_6, \quad t > 0,$$

and

$$\frac{\partial R_7}{\partial t} = \frac{D}{r^2}\frac{\partial}{\partial r}(r^2\frac{\partial R_7}{\partial r}) - \frac{\delta}{r^2}\frac{\partial}{\partial r}(r^2 R_7) - dR_7 - k_5 P R_7, \tag{4.2.7}$$

with boundary conditions

$$D\frac{\partial R_7}{\partial r}(r_1,t) - \delta R_7(r_1,t) = 0, \quad D\frac{\partial R_7}{\partial r}(r_2,t) - \delta R_7(r_2,t) = k_4' R_4 - k_{-4}' R_7, \quad t > 0.$$

4.2.2 Chico-PI3K complex subsystem

Chico is an insulin receptor substrate, which acts as a scaffold bringing together other molecules responsible for the signal. PI3Ks are a family of related intracellular signal transducer enzymes capable of phosphorylating the 3 position of a lipid when in a complex with Chico. Phosphorylated insulin-bound surface receptors phosphorylate Chico, leading to the Chico-PI3K complex in the cell, a product upstream of the activation of Akt and the deactivation of FOXO.

In this subsystem, the state variables are Chico:

$C_1(r,t)$, concentration of unphosphorylated Chico,

$C_2(t)$, concentration of phosphorylated Chico, and PI3K:

$\Phi_3(r,t)$, concentration of deactivated PI3K,

$\Xi(t)$, concentration of phosphorylated Chico-PI3K complex.

The synthesis of C_1: As with free receptors, the gene for Chico is transcribed in the nucleus and the RNA is translated to unphosphorylated Chico at a location contiguous to the nuclear membrane

from where it is actively transported to the cell membrane. At the cell membrane the phosphorylated surface receptors (R_3 and R_4) phosphorylate Chico according to a mass-action law with rate k_7. Also, phosphorylated Chico (C_2) is dephosphorylated by PTPases according to a mass-action reaction with rate k_{-7}. The basal transcription rate of unphosphorylated Chico is denoted by b_c and it degrades at a rate denoted by d_c. Therefore, the synthesis rate of unphosphorylated Chico is

$$\frac{\partial C_1}{\partial t} = \frac{D}{r^2}\frac{\partial}{\partial r}(r^2\frac{\partial C_1}{\partial r}) - \frac{\delta}{r^2}\frac{\partial}{\partial r}(r^2 C_1) - d_c C_1, \tag{4.2.8}$$

with boundary conditions

$$D\frac{\partial C_1}{\partial r}(r_1, t) - \delta C_1(r_1, t) = -b_c,$$
$$D\frac{\partial C_1}{\partial r}(r_2, t) - \delta C_1(r_2, t) = k_{-7}PC_2 - k_7 C_1(R_3 + R_4).$$

The synthesis of C_2: Phosphorylation of Chico by surface receptors (R_3 and R_4) is described above, as is its dephosphorylation by PTPases. Phosphorylated Chico (C_2) binds with deactivated PI3K (Φ_3) according to mass-action kinetics forming the Chico-PI3K complex (Ξ) at a rate denoted by k_8. The dissociation of the phosphorylated Chico-PI3K complex into its two components takes place at a rate denoted by k_{-8}. Phosphorylated Chico degrades at a rate denoted by d_c. Therefore, the synthesis rate of phosphorylated Chico is

$$\dot{C_2} = k_7 C_1(r_2, t)(R_3 + R_4) + k_{-8}\Xi - k_{-7}PC_2 - k_8\Phi_3(r_2, t)C_2 - d_c C_2. \tag{4.2.9}$$

The synthesis of Φ_3: This unphosphorylated PI3 kinase is translated adjacent to the nucleus from where it is transported to the cell membrane, as with other proteins described above. The basal transcription rate of unphosphorylated PI3K is denoted by b_p and the degradation rate is

denoted by d_p. As mentioned above the dissociation rate of the phosphorylated IRS-PI3K complex is denoted by k_{-8}. Therefore, the synthesis rate of unphosphorylated PI3K is

$$\frac{\partial \Phi_3}{\partial t} = \frac{D}{r^2}\frac{\partial}{\partial r}(r^2\frac{\partial \Phi_3}{\partial r}) - \frac{\delta}{r^2}\frac{\partial}{\partial r}(r^2\Phi_3) - d_p\Phi_3, \tag{4.2.10}$$

with boundary conditions

$$D\frac{\partial \Phi_3}{\partial r}(r_1,t) - \delta\Phi_3(r_1,t) = -b_p, \quad D\frac{\partial \Phi_3}{\partial r}(r_2,t) - \delta\Phi_3(r_2,t) = -k_8\Phi_3(r_2,t)C_2 + k_{-8}\Xi.$$

The synthesis of Ξ: As mentioned above, through a mass-action reaction the production rate of the phosphorylated Chico-PI3K complex is denoted by k_8 and the dissociation rate is denoted by k_{-8}. We use d_{pc} to denote the degradation rate of phosphorylated PI3K-Chico complex. Therefore, the synthesis rate of phosphorylated Chico-PI3K complex (Ξ) is

$$\dot{\Xi} = k_8C_2\Phi_3(r_2,t) - k_{-8}\Xi - d_{pc}\Xi. \tag{4.2.11}$$

4.2.3 Lipids subsystem

Adjacent to the cell membrane, the phosphorylated Chico-PI3K complex (Ξ) converts the substrate phosphatidylinositol 4,5-bisphosphate ($PI(4,5)P_2$) to the substrate product phosphatidylinositol 3,4,5-trisphosphate ($PI(3,4,5)P_3$). Furthermore, there is spontaneous phosphorylation and dephosphorylation giving transitions between these t-wo states and between $PI(3,4,5)P_3$) and another, $PI(3,4)P_2$. Some of these are catalyzed by PTEN and SHIP, whose concentrations we take to be constant and are implicitly included in the rate constants shown below. We assume that the total amount of PIP is conserved.

Let

$P_3(t)$ be the concentration of $PI(3,4,5)P_3$,

$P_4(t)$ be the concentration of $PI(3,4)P_2$,

$P_5(t)$ be the concentration of $PI(4,5)P_2$.

Notice that conservation gives $L \equiv P_3 + P_4 + P_5$. The equations to describe the synthesis rates of P_3, P_4 and P_5 are

$$\dot{P_3} = k_{9p}\Xi P_5 + k_{9b}P_5 + k_{10}P_4 - k_{-9}P_3 - k_{-10}P_3, \tag{4.2.12}$$

$$\dot{P_4} = k_{-10}P_3 - k_{10}P_4, \tag{4.2.13}$$

$$\dot{P_5} = k_{-9}P_3 - (k_{9p}\Xi + k_{9b})P_5. \tag{4.2.14}$$

4.2.4 Akt subsystem

Akt is also known as Protein Kinase B (PKB), and as this name suggests it is a (serine/threonine) protein kinase, that is, it acts as a catalyst for protein interactions. It is produced in the vicinity of the nucleus, in its inactive or unphosphorylated state from where it is actively transported to the cell membrane where it becomes phosphorylated by the lipid $PI(3,4,5)P_3$.

The state variables for Akt are denoted by:

$A(r,t)$, concentration of deactivated Akt,

$A_p(r,t)$, concentration of activated Akt.

The synthesis of A and A_p: The basal transcription to unphosphorylated Akt (A) is denoted by b_A and its degradation rate (decay constant) is denoted by d_A. We assume that the degradation of activated Akt (A_p) occurs at the same rate. The lipid $PI(3,4,5)P_3$ (P_3) phosphorylates inactive Akt

at a rate proportional to the concentrations of this lipid and of A with the rate constant denoted by k_{11}. Activated Akt is dephosphorylated spontaneously and becomes deactivated Akt with the rate k_{-11}. Also, activated Akt is transported from the cell membrane to the nucleus, where it interacts with activated FOXO, deactivating it through phosphorylation ([16]). Hence, the equations to describe the synthesis rates of A and A_p are

$$\frac{\partial A}{\partial t} = \frac{D}{r^2}\frac{\partial}{\partial r}(r^2\frac{\partial A}{\partial r}) - \frac{\delta}{r^2}\frac{\partial}{\partial r}(r^2 A) - d_A A + k_{-11}A_p, \tag{4.2.15}$$

with boundary conditions

$$D\frac{\partial A}{\partial r}(r_1,t) - \delta A(r_1,t) = -b_A, \quad D\frac{\partial A}{\partial r}(r_2,t) - \delta A(r_2,t) = -k_{11}A(r_2,t)P_3,$$

and

$$\frac{\partial A_p}{\partial t} = \frac{D}{r^2}\frac{\partial}{\partial r}(r^2\frac{\partial A_p}{\partial r}) + \frac{\delta}{r^2}\frac{\partial}{\partial r}(r^2 A_p) - d_A A_p - k_{-11}A_p, \tag{4.2.16}$$

with boundary conditions

$$D\frac{\partial A_p}{\partial r}(r_1,t) + \delta A_p(r_1,t) = 0, \quad D\frac{\partial A_p}{\partial r}(r_2,t) + \delta A_p(r_2,t) = k_{11}A(r_2,t)P_3.$$

4.2.5 FOXO subsystem

As indicated above, FOXO is a transcription factor, coding for insulin receptors among other proteins. Its active state is unphosphorylated but activated Akt phosphorylates FOXO, making it inactive ([5]). In its inactive state, FOXO leaves the nucleus and, while in the cytoplasm, spontaneously becomes unphosphorylated, and is transported back to the nucleus ([14]). We assume that both states of FOXO degrade in the cytoplasm at a common rate d_f (see [6]) and that active

FOXO has a basal transcription rate of b_F in the nucleus.

The state variable for FOXO are denoted by:

$F(r,t)$, concentration of activated FOXO,

$f(r,t)$, concentration of deactivated FOXO.

To model the process of Akt phosphorylating FOXO at the nuclear membrane, we notice that when activated Akt interacts with activated FOXO, a small amount of temporary complex $[AF]$ forms quickly. Then $[AF]$ degrades to free activated Akt and phosphorylated FOXO f.

Using the Michaelis-Menten formalism, assuming quasi steady state for this fast reaction, and ignoring higher order terms of small quantities, we find the production of phosphorylated FOXO f is proportional to the amount of [AF]:

$$k_{12}\frac{\beta A_p F}{(\beta+1)F + A_p},$$

where β is the ratio of the rate at which the $[AF]$ forms to the rate at which it dissociates.

We thus have the synthesis rates of F and f:

$$\frac{\partial F}{\partial t} = \frac{D}{r^2}\frac{\partial}{\partial r}(r^2\frac{\partial F}{\partial r}) + \frac{\delta}{r^2}\frac{\partial}{\partial r}(r^2 F) + k_{-12}f - d_f F, \tag{4.2.17}$$

with boundary condition

$$D\frac{\partial F}{\partial r}(r_1,t) + \delta F(r_1,t) = k_{12}\frac{\beta A_p F(r_1,t)}{(\beta+1)F(r_1,t) + A_p(r_1,t)} - b_F,$$

$$D\frac{\partial F}{\partial r}(r_2,t) + \delta F(r_2,t) = 0,$$

and

$$\frac{\partial f}{\partial t} = \frac{D}{r^2}\frac{\partial}{\partial r}(r^2\frac{\partial f}{\partial r}) - \frac{\delta}{r^2}\frac{\partial}{\partial r}(r^2 f) - k_{-12}f - d_f f, \tag{4.2.18}$$

with boundary condition

$$D\frac{\partial f}{\partial r}(r_1, t) - \delta f(r_1, t) = -k_{12}\frac{\beta A_p F(r_1, t)}{(\beta + 1)F(r_1, t) + A_p(r_1, t)},$$

$$D\frac{\partial f}{\partial r}(r_2, t) - \delta f(r_2, t) = 0.$$

4.2.6 PTPases

In the model in [11], the activity of PTPases, P, is described as a piecewise linear function of the percentage of activated Akt (the ratio of activated Akt over total Akt) in such a way that P degenerates to zero when the percentage of activated Akt exceeds 36.4%, in accordance with experimental data. To get smoothness of $P(r, t)$, we use an exponential function instead to model the activity of PTPases:

$$P(r, t) = e^{-kA_p(r,t)}, \tag{4.2.19}$$

where the coefficient k is chosen by fitting to the piecewise linear function above.

4.3 The results

It is possible to show that the large system of reaction-diffusion equations coupled to ODE's through boundary values has a unique solution, existing for all time, at least for nonnegative initial data. However, the point of interest here is the qualitative behavior of solutions, and in particular, whether or not the system reproduces experimental data. We will also be interested in the evolution

of the pathway and to what extent it is robust and optimized in some sense. These will be topics of further study. The results we report here are twofold.

Fist of all, the insulin signalling leads to a reduction in activated FOXO. The insulin (or more generally, insulin-like) signalling pathway regulates the growth of the cell through the negative growth regulator, FOXO. Specifically, developmental nutrition leads to the release of insulin-like peptides in the blood stream. When insulin is high, FOXO is phosphorylated downstream along the IIS pathway. This disrupts DNA binding and causes FOXO to translocate to the cytoplasm. A decline in insulin leads to an accumulation of active FOXO in the nucleus, increasing the transcription of growth inhibitors. Also, the transcription of insulin receptors increases, which strengthens the insulin signal and thus moderates the increase of growth inhibitors. In the figure 2, we vary the concentration of model input–insulin and look at the concentration of activated FOXO in the nucleus at 10 minutes ($F(r_1, 10)$). The concentration of activated FOXO decreases as the concentration of insulin increases. This agrees with our understanding of the IIS pathway.

Secondly, the sensitivity of activated FOXO is regulated by the expression of total FOXO. For animals, all the organs of an individual share the same structure of IIS pathway. However, not all organs show the same growth response to changes in developmental nutrition. For instance, in the fruit fly, *Drosophila melanogaster*, a reduction in developmental nutrition has more of an effect on wing size than on genital size, and this is a consequence of genital growth being less sensitive to changes in IIS. Similarly, in mammals the developing brain is relatively insensitive to changes in nutrition, a phenomenon called head sparing. Such organ-specific differences in nutritional- and insulin-sensitivity is fundamental to ensure that final body proportion is correct across a range of adult sizes.

Work on *Drosophila melanogaster* has revealed that the reduced insulin-sensitivity of the genitalia is a consequence of changes in the expression of key genes in the IIS pathway, specifically

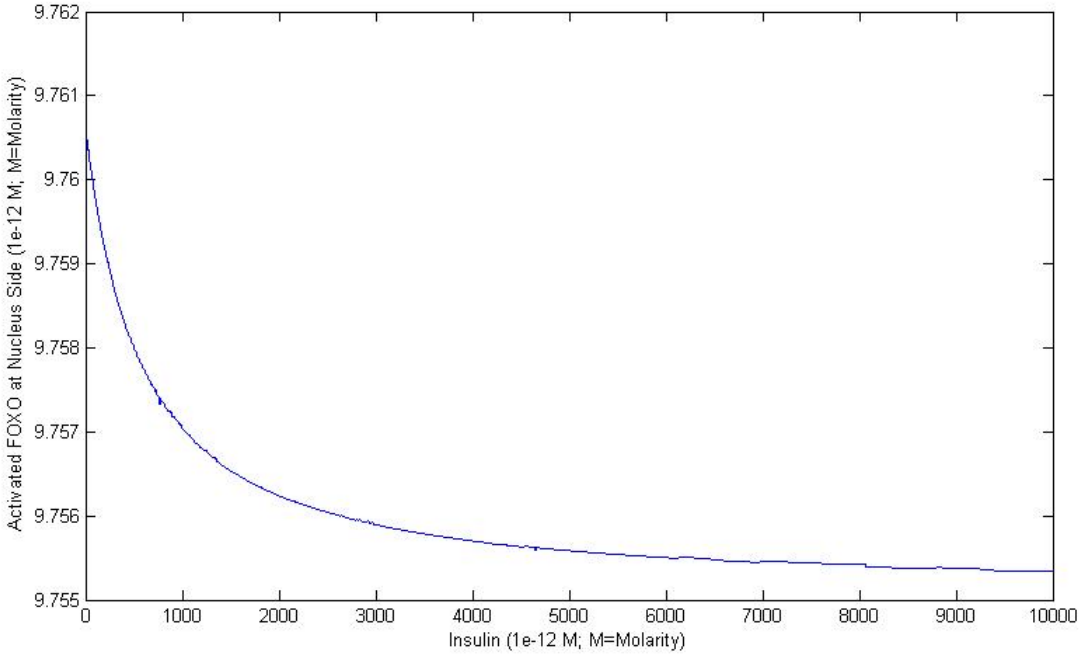

Figure 4.2: Nuclear FOXO vs. Insulin

the forkhead transcription factor FOXO ([15]). In order to verify the hypothesis with our model, we define the Sensitivity of Activated FOXO as the differences of the concentration of activated FOXO in the nucleus ($F(r_1, 10)$) at two insulin levels:

$$\text{Sensitivity} = F(r_1, 10; I_1) - F(r_1, 10; I_2)$$

where the two insulin levels are $I_1 = 1$ picomol and $I_2 = 10^5$ picomol.

Then by fixing the degradation rate of activated FOXO and manipulating the basal transcription rate, we change the expression of FOXO. Consequently, the sensitivity of activated FOXO is a function of the basal transcription rate. In Figure 3, the simulation shows that the sensitivity of activated FOXO increases as the basal transcription rate increases from 0 to 10 picomolar/min. Thus the sensitivity of activated FOXO to the signal from the IIS pathway is manipulated by the expression of FOXO itself, which verifies our hypothesis.

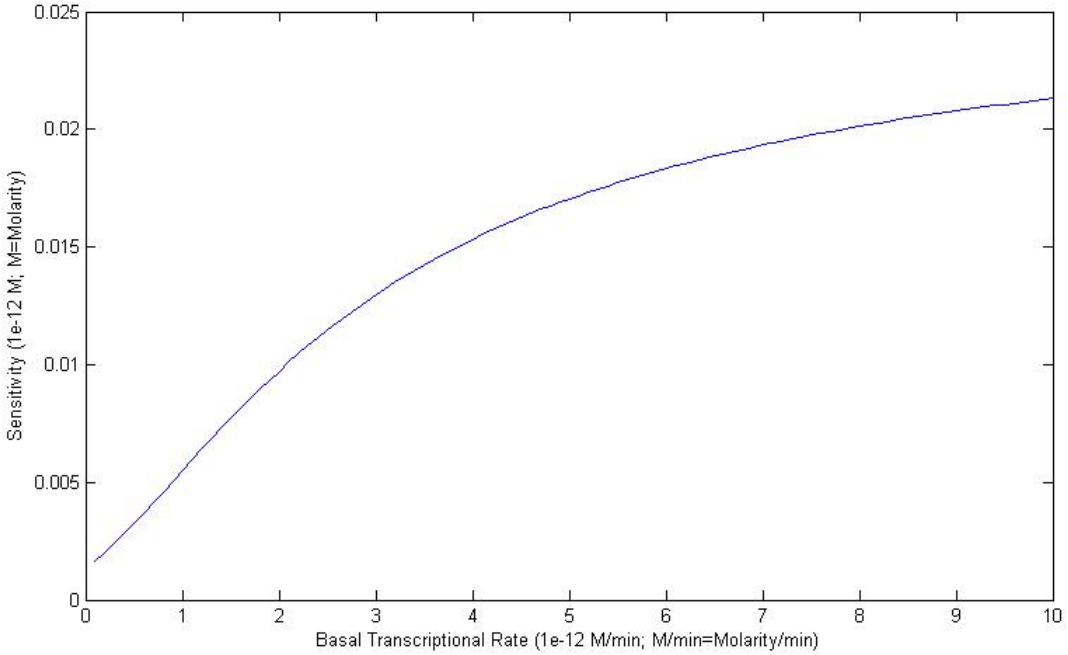

Figure 4.3: The Sensitivity of Activated FOXO

4.4 Model coefficients

The prefactor k in the exponent of the equation of PTP was taken to be 0.03 based on the observation that activated Akt inhibits the action of PTP1B with a 25% decrease after maximal insulin stimulation. The ratio of activated Akt to deactivated Akt is 1:10 after the maximal insulin simulation ([11]) and the total steady state amount of Akt is taken to be $100pM$, and so from the equation of PTP k should be $0.11 * \log \frac{4}{3}$. The radius of cell, r_2, was chosen to be 6 μm based on experimental data that gives the cross-sectional area of *Drosophila* wing cells ranging from 87.59 μm^2 to 279.83 μm^2 ([10]). Assuming the radius of a cell nucleus is half that of the cell, which is common, we took r_1 to be 3 μm. We performed simulations with other values of r_1 and r_2 giving very similar results. In ([1]), transport by molecular motors is given as being around 800 $nm \cdot sec^{-1}$ which is about 50 $\mu m \cdot min^{-1}$. Thus, we took δ to be 50. We took D to be 25, equivalent to assuming that 5% of the molecules are transported by diffusion. The rate of feedback, γ, from activated

FOXO to insulin receptors is unknown and we took it to be unity. Other unknown parameters, taken to be unity for lack of experimatal data, include α, the affinity coefficient of the activated FOXO binding with the DNA, β, the affinity coefficient for activated Akt binding with activated FOXO, k_{12}, the other parameter in the Michaelis-Menten reaction deactivating FOXO, and k_{-12} the rate at which deactivated FOXO is dephosphorylated in the cytoplasm, thus returning to its active state. The degradation coefficients are assumed to be 0.1 min^{-1} and the basal transcripiton constants ranging from 0 to 10 $pM \cdot min^{-1}$ were based on the initial conditions of the molecular concentrations in the original ODE model ([11]).

Here are the lists of the variable in the partial differential equations:

$R_1(t)$: the concentration of unbound unphosphorylated cell-surface receptors;

$R_2(t)$: the concentration of once-bound unphosphorylated cell-surface receptors;

$R_3(t)$: the concentration of phosphorylated twice-bound cell-surface receptors;

$R_4(t)$: the concentration of phosphorylated once-bound cell-surface receptors;

$R_5(r,t)$: the concentration of unbound unphosphorylated intracellular receptors;

$R_6(r,t)$: the concentration of phosphorylated twice-bound intracellular receptors;

$R_7(r,t)$: the concentration of phosphorylated once-bound intracellular receptors;

$P(r,t)$: a prefactor representing the relative activity of PTPases;

$C_1(r,t)$: the concentration of unphosphorylated Chico;

$C_2(t)$: the concentration of phosphorylated Chico;

$\Phi_3(r,t)$: the concentration of deactivated PI3K;

$\Xi(t)$: the concentration of phosphorylated Chico-PI3K complex;

$P_3(t)$: the concentration of $PI(3,4,5)P_3$;

$P_4(t)$: the concentration of $PI(3,4)P_2$;

$P_5(t)$: the concentration of $PI(4,5)P_2$;

$A(r,t)$: the concentration of deactivated Akt;

$A_p(r,t)$: the concentration of activated Akt;

$F(r,t)$: the concentration of activated FOXO;

$f(r,t)$: the concentration of deactivated FOXO.

The coefficients that are taken from [11] are (pM = picomolar and μm = micrometer):

$k_1 = 6 \times 10^{-5} pM^{-1} \cdot min^{-1}$;

$k_{-1} = 0.2 min^{-1}$;

$k_2 = k_1 min^{-1}$;

$k_{-2} = 20 min^{-1}$;

$k_3 = 2500 min^{-1}$;

$k_{-3} = 0.2 min^{-1}$;

$k_4 = 0.0003 min^{-1}$;

$k_{-4} = 0.003 min^{-1}$;

$k_{4'} = 2.1 \times 10^{-3} min^{-1}$;

$k_{-4'} = 2.1 \times 10^{-4} min^{-1}$;

$k_6 = 0.461 min^{-1}$;

$k_7 = 4.638 min^{-1}$;

$k_{-7} = 1.396 min^{-1}$;

$k_8 = 0.707 pM^{-1} \cdot min^{-1}$;

$k_{-8} = 10 min^{-1}$;

$k_{-9} = 42.148 min^{-1}$;

$k_{9b} = 0.131 min^{-1}$;

$k_{9p} = 1.390 min^{-1}$;

$k_{10} = 2.961 min^{-1}$;

$k_{-10} = 2.77 min^{-1}$;

$k_{11} = 2.484 min^{-1}$;

$k_{-11} = 6.932 min^{-1}$.

The new coefficients of the ordinary differential equations are:

$r_1 = 3\mu m$;

$r_2 = 6\mu m$;

$D = 25\mu m^2 \cdot min^{-1}$;

$\delta = 50\mu m \cdot min^{-1}$;

$k = 0.03$;

$k_{12} = 30 pM^{-1} \cdot min^{-1}$;

$k_{-12} = 1 min^{-1}$;

$\alpha = 1$;

$\beta = 2$;

$d_5 = 0.1 min^{-1}$;

$d_c = 0.1 min^{-1}$;

$d_p = 0.1 min^{-1}$;

$d_{pc} = 0.1 min^{-1}$;

$d_A = 0.1 min^{-1}$;

$d_f = 0.1 min^{-1}$;

$b_5 = 1 pM \cdot min^{-1}$;

$b_c = 1 pM \cdot min^{-1}$;

$b_p = 1 pM \cdot min^{-1}$;

$b_a = 1 pM \cdot min^{-1}$;

$b_F = 1 pM \cdot min^{-1}$.

Chapter 5

The bifurcations of a nonlocal Chafee-Infante problem

5.1 Introduction

In the second part of the thesis, I consider the nonlocal diffusion equation:

$$L_\epsilon u + \lambda(u - u^3) = 0.$$

where $L_\epsilon u$ is an integral defined as

$$L_\epsilon u = \int_0^\pi \epsilon^{-3} J(\frac{y-x}{\epsilon})(u(y) - u(x))dy.$$

Bates and Zhao study the spectra of this operator. It is shown that as the scaling parameter ϵ tends to zero, the spectrum of the nonlocal operator converge to the spectrum of the Laplace operator with Neumann boundary condition ([26]). Hence, when ϵ is small, one may compare the above nonlocal diffusion equation with the steady states of the Chafee-Infante equation:

$$\begin{cases} u_{xx} + \lambda(u - u^3) = 0, \quad in \quad 0 < x < \pi, \\ u'(0) = 0, \quad u'(\pi) = 0. \end{cases}$$

It is known that the Chafee-Infante equation has global bifurcations. The trivial solution of constant zero bifurcates when λ equal to the spectrum of the Laplace operator with Neumann boundary condition ([30]). The natural question is whether the nonlocal operator has the similar bifurcation properties as the Chafee-Infante problem. In chapter five of the thesis, it is shown that as the scaling parameter ϵ approaches zero, the nonlocal diffusion equation has the local pitchfork bifurcation at the spectrum of the nonlocal operator L_ϵ. In the later part of this chapter, a concrete example is discussed. For a concrete kernel, I solve the nonlocal diffusion equation with the Newton's Method and the first, second and third bifurcation diagrams are plotted. For the concrete example, the bifurcations of the nonlocal diffusion equation fail to be global. To show that, the case with λ being large is consider. It is shown that as the parameter λ is large, the solution on the first bifurcation branch has a jump discontinuity.

5.2 The local bifurcation

Let Ω be an open set with smooth boundary on R^n. Define a nonlocal operator L_ϵ on the Hilbert space $L^2(\Omega)$ as follows:

$$(L_\epsilon \omega)(x) = \int_\Omega \epsilon^{-2} J_\epsilon(x-y)[\omega(y) - \omega(x)]dy.$$

where $\epsilon > 0$, $J_\epsilon(x-y) = \epsilon^{-n} J(\frac{x-y}{\epsilon})$ and $J(\cdot) \in C_c(R^n)$ with $suppJ \subset B_R$, $B_R = \{x \in R^n :\mid x \mid \leq R\}, J \geq 0, J(z) = J(\mid z \mid)$. It is easy to verify that L_ϵ is a bounded linear operator on $L^2(\Omega)$.

In this paper, we are looking for the bifurcation points of the following equation:

$$L_\epsilon u + \lambda(u - u^3) = 0, \quad in \quad \Omega \tag{5.2.1}$$

where $\lambda \in R$ is the parameter.

This equation can also be formulated to a functional equation:

$$G(\lambda, u) = 0 \tag{5.2.2}$$

where $G : R \times X \mapsto X$, $X = L^2(\Omega)$ is a Banach space.

Notice that $G_u(\lambda, 0) = L_\epsilon + \lambda$ and $(\lambda, 0)$ is the trivial solution of the nonlocal diffusion equation. Inspired by the implicit function theorem, we investigate the spectrum of the operator L_ϵ, i.e. where $G_u(\lambda, 0)$ is not invertible. In fact, at λ where $G_u(\lambda, 0)$ has finite dimensional kernel, $G_u(\lambda, 0)$ is a Fredholm operator.

Lemma 5.2.1. *Assume $\lambda \in \sigma(L_\epsilon)$ and $dim(N(G_u(\lambda, 0))) < \infty$, then $G_u(\lambda, 0)$ is a Fredholm operator with index zero.*

Proof. One can verify that $G_u(\lambda, 0) = L_\epsilon + \lambda$ is a self-adjoint operator on $L^2(\Omega)$. In fact,

$$\begin{aligned}
&((L_\epsilon + \lambda)u, v) \\
&= \int_\Omega (L_\epsilon + \lambda)uvdx \\
&= \int_\Omega L_\epsilon uvdx + \int_\Omega \lambda uvdx \\
&= \int_\Omega \int_\Omega \epsilon^{-2} J_\epsilon(x-y)(u(y)-u(x))v(x)dydx + \int_\Omega \lambda uvdx \\
&= \int_\Omega \int_\Omega \epsilon^{-2} J_\epsilon(x-y)u(y)v(x)dydx - \int_\Omega \int_\Omega \epsilon^{-2} J_\epsilon(x-y)u(x)v(x)dydx + \int_\Omega \lambda uvdx \\
&= \int_\Omega \int_\Omega \epsilon^{-2} J_\epsilon(x-y)u(x)v(y)dydx - \int_\Omega \int_\Omega \epsilon^{-2} J_\epsilon(x-y)u(x)v(x)dydx + \int_\Omega \lambda uvdx \\
&= \int_\Omega \int_\Omega \epsilon^{-2} J_\epsilon(x-y)(v(y)-v(x))u(x)dydx + \int_\Omega \lambda uvdx \\
&= ((L_\epsilon + \lambda)v, u).
\end{aligned} \tag{5.2.3}$$

Thus, $G_u(\lambda, 0)$ is a self-adjoint bounded linear operator on Hilbert space $L^2(\Omega)$, $N(G_u(\lambda, 0)) = N(G_u^*(\lambda, 0)) = (Range(G_u(\lambda, 0)))^{\perp}$. Hence, $codim(Range(G_u(\lambda, 0))) = dim(N(G_u(\lambda, 0)))$.

In addition, $Range(G_u(\lambda, 0))$ is closed. Indeed, $G_u(\lambda, 0)$ has a finite dimensional kernel. So $N(G_u(\lambda, 0))$ is closed and $L^2(\Omega)/ker(G_u(\lambda, 0))$ is a Banach space. Define the map

$$S : L^2(\Omega)/ker(G_u(\lambda, 0)) \bigoplus (Range(G_u(\lambda, 0)))^{\perp} \to L^2(\Omega)$$

to be: $S(x, c) = T(x) + c$. Then, S is a bounded linear isomorphism. Hence by open mapping theorem, it is a topological isomorphism. Thus, $Range(G_u(\lambda, 0)) \cong L^2(\Omega)/ker(G_u(\lambda, 0)) \bigoplus \{0\}$ and $Range(G_u(\lambda, 0))$ is closed.

Therefore, $G_u(\lambda, 0)$ is a Fredholm operator with index zero.

□

Let $\triangle^N : D(\triangle^N) \subset L^2(\Omega) \mapsto L^2(\Omega)$ be the Neumann realization of the Lapacian in Ω defined by

$$D(\triangle^N) = \{u \in H^2(\Omega) : \frac{\partial u}{\partial \nu} = 0, \quad on \quad \partial\Omega\}$$

where $\triangle^N u = \triangle u = \sum_{i=1}^n \frac{\partial^2 u}{\partial x_i^2}$, $u \in D(\triangle^N)$ and $\nu = (\nu_1, ..., \nu_n)$ is outward normal unit vector to the boundary $\partial\Omega$.

Then we rewrite the following equation:

$$\begin{cases} c_J \triangle u + \lambda u = 0, \quad in \quad \Omega \\ \frac{\partial u}{\partial \nu} = 0, \quad on \quad \partial\Omega \end{cases}$$

$c_J = \frac{1}{2}\int_{R^n} J(z) \mid z \mid^2 dz$. in an abstract way:

$$F(\lambda, u) = 0 \tag{5.2.4}$$

where $F : R \times D(\triangle^N) \mapsto L^2(\Omega)$ is a mapping.

By ([26]), on any bounded close set, the spectrum of the operator $G_u(\lambda, 0)$ converges to the spectrum of $F(\lambda, u)$ as ϵ is sufficiently small. Hence, we analyse the bifurcation properties of equation G around any bifurcation points $(\mu, 0)$ of the equation F. And we have the following theorem:

Theorem 5.2.2. *Suppose that $-\mu \in \sigma(c_J\triangle^N)$ is a simple eigenvalue of $c_J\triangle^N$. And let $B_\delta(\mu) = \{\lambda \in C :\mid \lambda - \mu \mid\leq \delta\}$ with $\delta > 0$ so small that $B_\delta \cap \sigma(c_J\triangle^N) = \{-\mu\}$. Then (a), there exists $\epsilon > 0$ so that when ϵ is sufficiently small $B_\delta \cap \sigma(L_\epsilon) = \{-\lambda_0\}$ and $-\lambda_0$ is a simple eigenvalue of L_ϵ. (b), if we assume $N(G_u(\lambda, 0)) = span\{\omega_0\}$ and Z be any complement of $N(G_u(\lambda, 0))$ in $L^2(\Omega)$, then the solution set of $G(\lambda, u) = 0$ near $(\lambda_0, 0)$ consists precisely of the curves $u = 0$ and $\{(\lambda(s), u(s)) : s \in I = (-a, a)\}$, where $\lambda : I \mapsto \mathbb{R}$ is a C^2 function and $z : I \mapsto Z$ is a C^1 function such that $u(s) = s\omega_0 + sz(s)$, $\lambda(0) = \lambda_0$, $z(0) = 0$ and $\lambda^{'}(0) = \lambda^{''}(0) = 0$.*

Proof. According to the theorem 2.1 of [26], we have part (a) that $-\lambda_0$ is a simple eigenvalue of L_ϵ. By Lemma 5.2.1, $G_u(\lambda, 0)$ is a Fredholm operator with index 0, i.e $dim(N(G_u(\lambda, 0))) = codim(R(G_u(\lambda, 0))) = 1$. $G_u(\lambda, 0)$ is an isomorphism from Z to $R(G_u(\lambda, 0))$.

We apply the Lyapunov-Schmidt process, denoting Q as the projection from $L^2(\Omega)$ into $R(G_u(\lambda, 0))$. Then $G(\lambda, u) = 0$ is equivalent to $Q \circ G(\lambda, u) = 0$ and $(I - Q) \circ G(\lambda, u) = 0$.

Define that:

$$f(\lambda, t, g) = Q \circ G(\lambda, t\omega_0 + g) = 0$$

where $t \in \mathbb{R}$ and $g \in Z$. Calculation shows that $f_g(\lambda, 0, 0) = Q \circ G_u(\lambda, 0)$, which is an isomorphism from Z to $R(G_u(\lambda, 0))$. Hence, by the implicit function theorem, for (λ, t) near $(\lambda_0, 0)$, there exists $g = g(\lambda, t) \in C^2$ such that $f(\lambda, t, g)) = 0$. Since the $codim(R(G_u(\lambda, 0))) = 1$, there exist $l \in (L^2(\Omega))^*$ such that $R(G_u(\lambda, 0)) = \{v \in L^2(\Omega) :< l, v >= 0\}$. Thus, $u = t\omega_0 + g(\lambda, t)$ is the solution of $Q \circ G_u(\lambda, 0) = 0$ if and only if $(I - Q) \circ G(\lambda, t\omega + g(\lambda, t)) = 0$, i.e., the scalar equation $< l, G(\lambda, t\omega + g(\lambda, t)) >= 0$.

Notice that

$$f(\lambda, t, g(\lambda, t)) = Q \circ G(\lambda, t\omega_0 + g(\lambda, t)) = 0$$

is true for all (λ, t) near $(\lambda_0, 0)$. Differentiating f and evaluating at $(\lambda_0, 0)$, we obtain

$$0 = \nabla f = (Q \circ (G_\lambda + G_u[g_\lambda]), Q \circ G_u[\omega_0 + g_t])$$

Since $(\lambda, 0)$ are the trivial solutions of the nonlocal diffusion equation, $G_\lambda(\lambda_0, 0) = 0$ and $G_u(\lambda, 0)$ is an isomorphism from Z to $R(G_u(\lambda, 0))$, we can conclude that $g_t(\lambda_0, 0) = g_\lambda(\lambda_0, 0) = 0$.

Define $h(\lambda, t) =< l, G(\lambda, t\omega + g(\lambda, t)) >$, we can apply Theorem 2.1 of [32] to h.

$$\nabla h(\lambda_0, 0) = (h_\lambda, h_t) = (< l, G_\lambda + G_u[g_\lambda] >, < l, G_u[\omega_0 + g_t] >) = (0, 0).$$

For the Hessian matirx, we have

$$Hess(h) = \begin{pmatrix} h_{\lambda\lambda} & h_{\lambda t} \\ h_{t\lambda} & h_{tt} \end{pmatrix}$$

where

$$h_{t\lambda} = h_{\lambda t} =< l, G_{\lambda u}[\omega_0 + g_t] + G_{uu}[\omega_0 + g_t, g_\lambda + G_u[g_{\lambda t}]] >=< l, G_{\lambda u}[\omega_0] >;$$

$$h_{\lambda\lambda} =< l, G_{\lambda\lambda} + 2G_{\lambda u}[g_\lambda] + G_{uu}[g_\lambda, g_\lambda] + G_u[g_{\lambda\lambda}] >=< l, 0 >= 0;$$

$$h_{tt} =< l, G_{uu}[\omega_0 + g_t, \omega_0 + g_t] + G_u[g_{tt}] >=< l, G_{uu}[\omega_0, \omega_0] > .$$

In summary,

$$Hess(h) = \begin{pmatrix} 0 & < l, G_{\lambda u}[\omega_0] > \\ < l, G_{\lambda u}[\omega_0] > & < l, G_{uu}[\omega_0, \omega_0] > \end{pmatrix}.$$

For the determinant, we have $detHess(h) = - < l, G_{\lambda u}[\omega_0] >^2 < 0$. By theorem 2.1 of [31], the solution set of $G(\lambda, u) = 0$ near $(\lambda_0, 0)$ is a pair of intersection curves, $(\lambda_i(s), u_i(s)) = (\lambda_i(s), t_i(s)\omega_0 + g(\lambda_i(s), u_i(s)))$, with $i = 1, 2$. where $v_i = (\lambda_i^{'}(0), t_i^{'}(0))$ are the solution of

$$2 < l, G_{\lambda u}[\omega_0] >^2 v_1 v_2 + < l, G_{uu}[\omega_0, \omega_0] > v_2^2 = 0.$$

The solution $(v_1, v_2) = (1, 0)$ correspond to the line of trivial solutions and the solution $(v_1, v_2) = (0, 1)$ gives the $\lambda^{'}(0) = 0$.

□

5.3 A concrete example

We consider a concrete example. Let the dimension n equal to 1 and define the kernel $J(x)$ as follows:

$$J(x) = \begin{cases} 0; & x < -1 \\ {c_j}^{-1} cos(\frac{\pi x}{2}); & -1 \leq x \leq 1 \\ 0; & x > 1 \end{cases}$$

with $c_j = \frac{1}{2}\int_{-1}^{1} cos(\frac{\pi x}{2}) x^2 \, \mathrm{d}x$. $J(x)$ is a positive even function. It is a cosine function when x is within the interval $(-1, 1)$ and 0 otherwise.

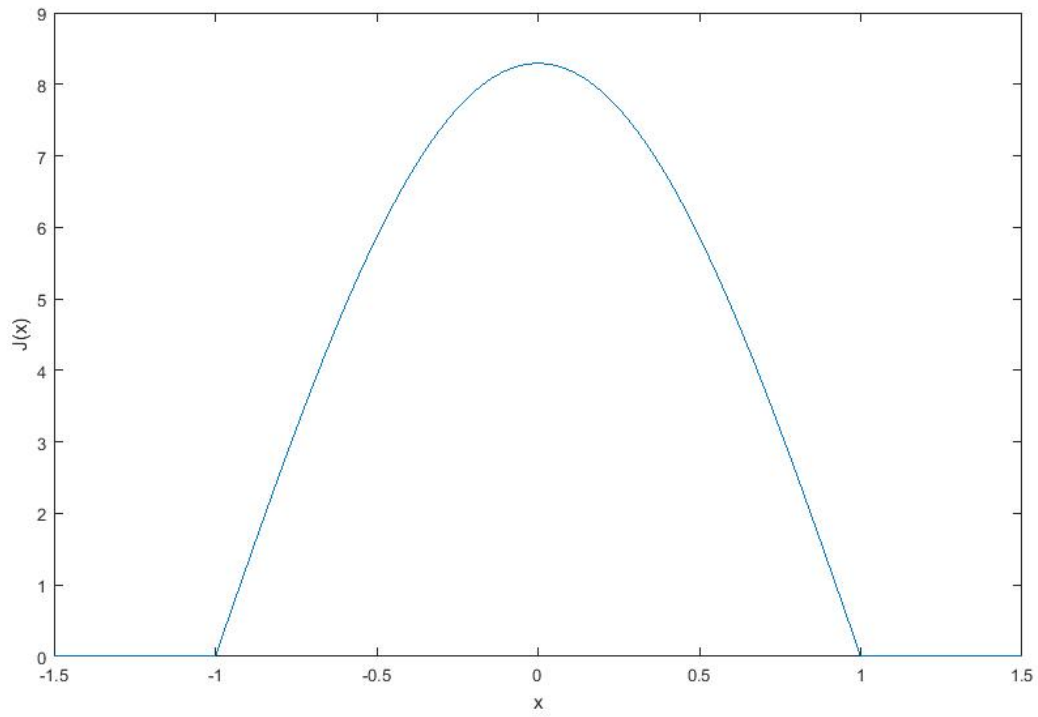

Figure 5.1: The kernel function $J(x)$.

Hence, we have the following one dimensional nonlocal integral equation:

$$G^{\epsilon}(\lambda, u) = L_{\epsilon}u + \lambda(u - u^3) = \epsilon^{-2} \int_0^{\pi} J_{\epsilon}(y - x)(u(y) - u(x))\,\mathrm{d}y + \lambda(u(x) - u(x)^3) = 0 \qquad (5.3.1)$$

By the mathematical analysis of the above section, when the scaling parameter ϵ is small, $G^{\epsilon}(\lambda, u)$ has the pitchfork bifurcation at $\lambda = n^2$ with n being the positive integer. We apply the Newton's method to find the solution of the equation on its first bifurcation branch. Specifically, we take the initial guess to be the function $u_0^{\epsilon} = tanh(\sqrt{\frac{\lambda}{2}}(x - \frac{\pi}{2}))$ and apply the Newton's iteration:

$$u_{n+1}^{\epsilon} = u_n^{\epsilon} - G_u^{\epsilon}(\lambda, u_n)^{-1} \circ G^{\epsilon}(\lambda, u_n)$$

where $\{u_n\}$ is the convergent sequence generated by the Newton's Method.

With ϵ to be 0.02 and λ to be 1, 2, 3 and 4 respectively, we get the simulations (figure 5.1).

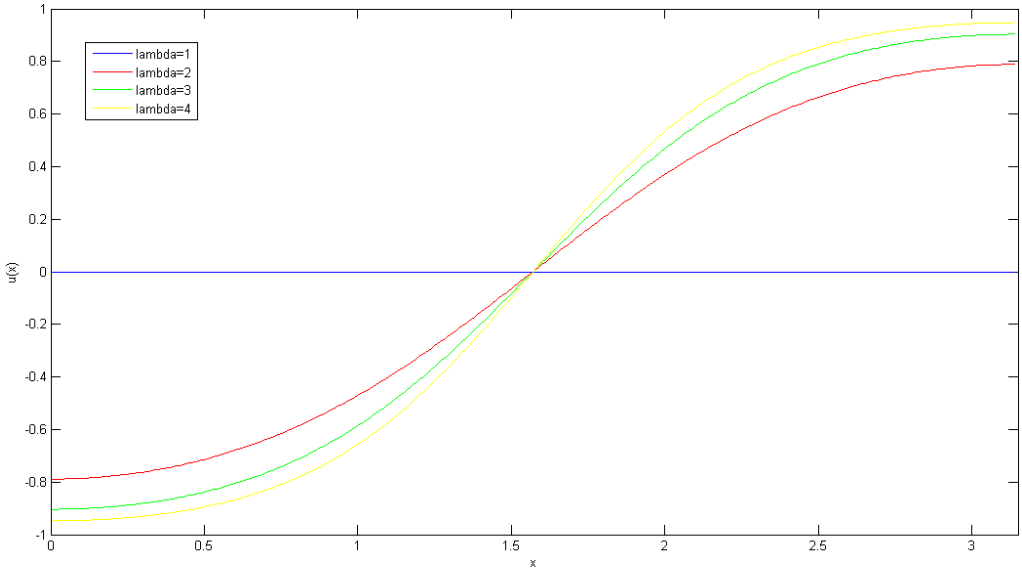

Figure 5.2: solutions of the nonlocal equation

In the simulations of figure 5.2, the blue curve stands for the solutions when $\lambda = 1$, which is

a trivial solution 0. The red curve stands for the solution when λ is 2. The green curve stands for the solution when λ is 3; the yellow curve stands for the solution when λ is 4. As λ increases, the solution $u^{\epsilon}(x)$ bifurcates from the trivial solution 0 and $\|u\|_{L_\infty(0,\pi)}$ increases from 0 to 1.

We known that the spectra of such nonlocal operators converge to the spectrum of a Laplace operator with the Neumann boundary condition as the scaling parameter ϵ tends to zero. Thus, we want to know if the solutions of the nonlocal diffusion equation is, to some extent, close to the Chafee-Infante problem. Hence, we solve the one dimensional Chafee-Infante problem with the boundary condition below by the Newton's Method as well and compare them with the nonlocal diffusion equation.

$$\begin{cases} u_{xx} + \lambda(u - u^3) = 0, \quad in \quad 0 < x < \pi, \\ u'(0) = 0, \quad u'(\pi) = 0. \end{cases}$$

In figure 5.3, figure 5.4, and figure 5.5, the red curves stand for the integral equations and the blue curves stand for the Chafee-Infante equation. Those simulations show that when the scaling parameter of the nonlocal diffuison equation ϵ is 0.02, for various λ values, the solutions of the nonlocal diffusion equation are very close to the solutions of the Chafee-Infante equation.

Furthermore, we would like to see the bifurcation diagrams of the nonlocal diffusion equation. It is well known that the solutions of the Chafee-Infante equation bifurcate at n^2. Inspired by figure 5.2, we modified the initial value of the Newton's method and find another two bifurcation points of the nonlocal diffusion equation.

The figure 5.6, figure 5.7, and figure 5.8 show that the nonlocal diffusion equation has the pitch-fork bifurcation at points around 1, 4, and 9, which verify the hypothesis that when ϵ is approaching zero, the bifurcation points of the nonlocal diffusion equation converges to the bifurcation points

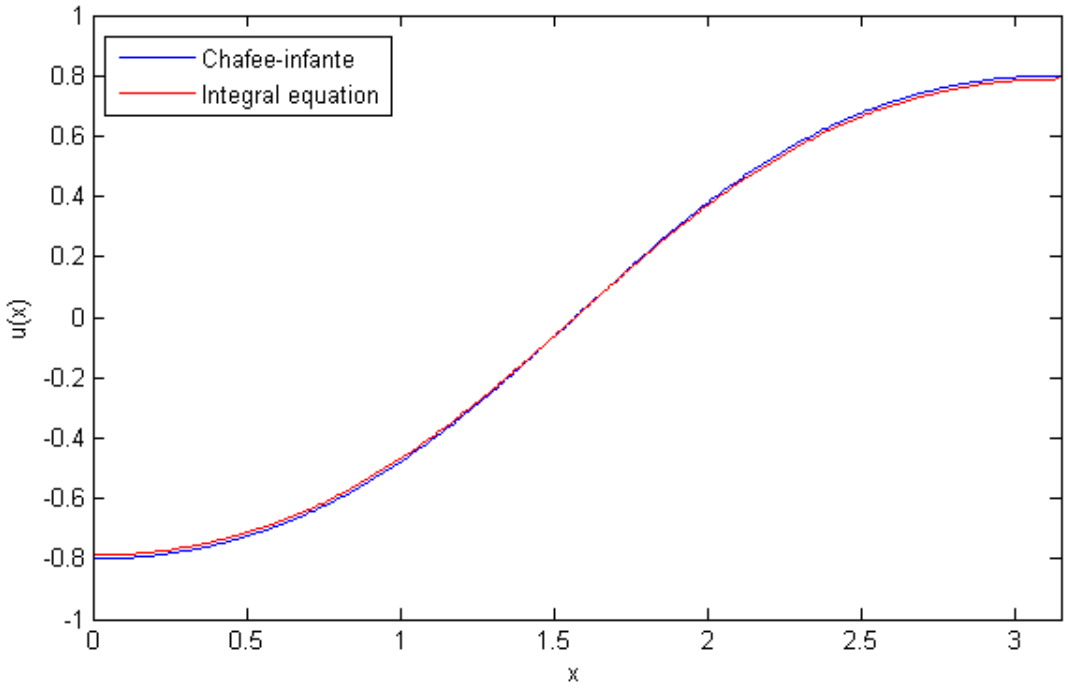

Figure 5.3: Comparison of the solutions of the nonlocal equation with $\lambda = 2$ and the Chafee-Infante equation.

of the Chafee-Infante equation.

In figure 5.9, the three dimensional graph shows how the solutions of the nonlocal diffusion equation on the first bifurcation branch vary as the parameter λ increase from 0 to 20. When λ is less than a point close to 1, solutions of the nonlocal diffusion equation are constant. When λ is greater than the first bifurcation point, there are non-constant increasing odd solutions. The L_∞ norm of those solutions increase as λ increases.

Figure 5.10 shows the extreme case that when λ is 10000. When λ is 10000, the simulation shows that a non-trivial solution of the nonlocal diffuison equation exists and it is a discontinuous function with a jump discontinuity at $x = 0$.

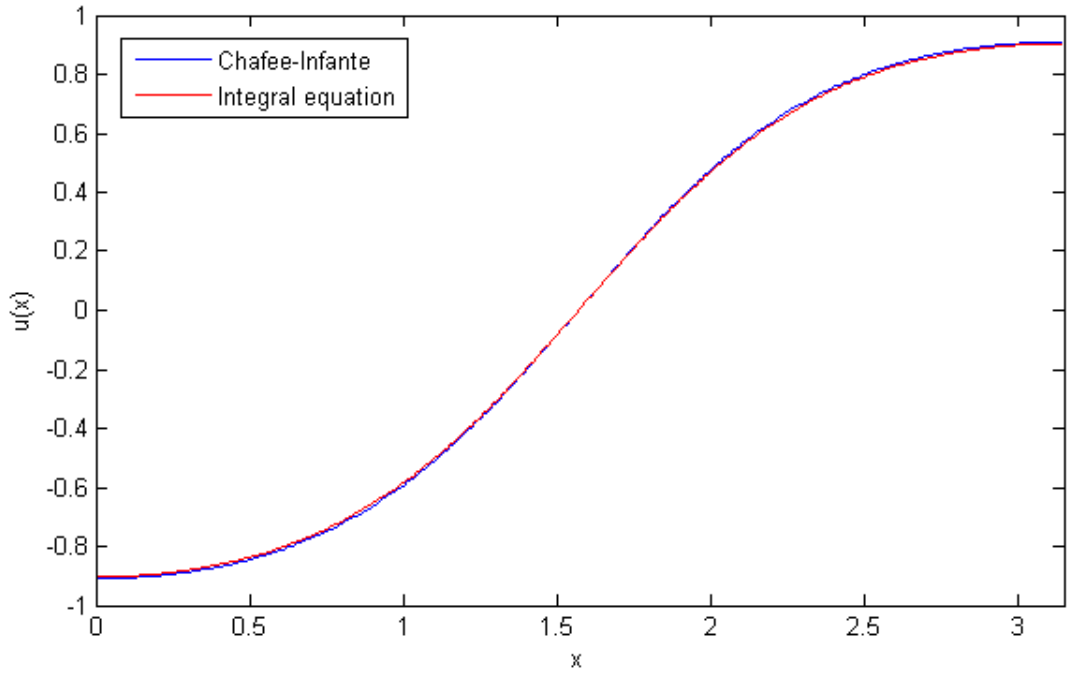

Figure 5.4: Comparison of the solutions of the nonlocal equation with $\lambda = 3$ and the Chafee-Infante equation.

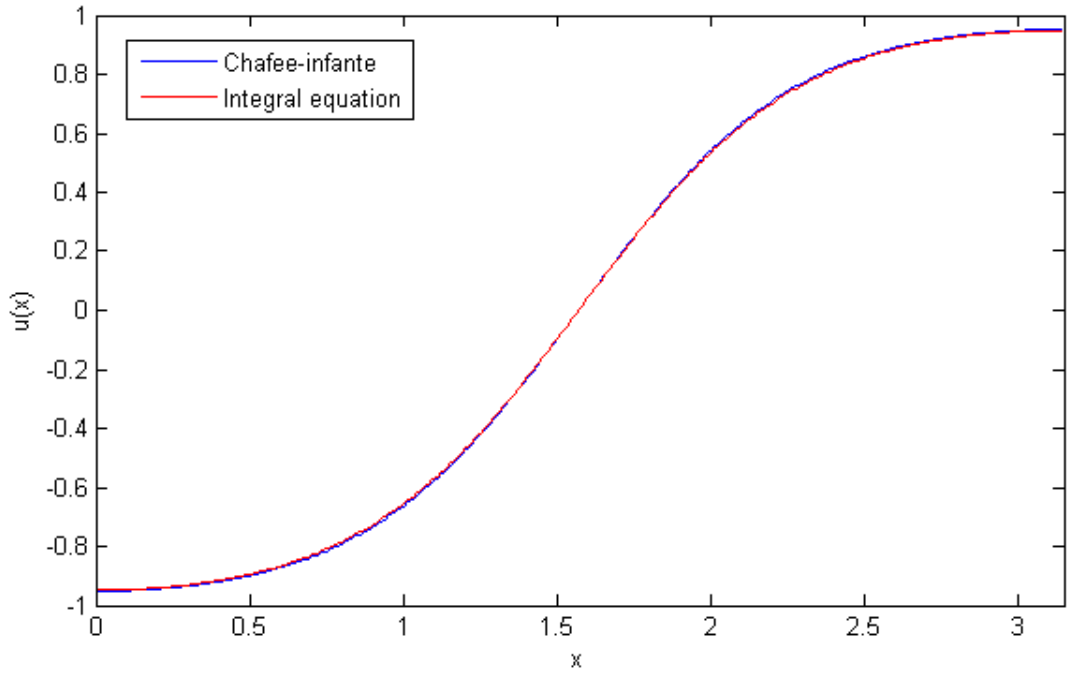

Figure 5.5: Comparison of the solutions of the nonlocal equation with $\lambda = 4$ and the Chafee-Infante equation.

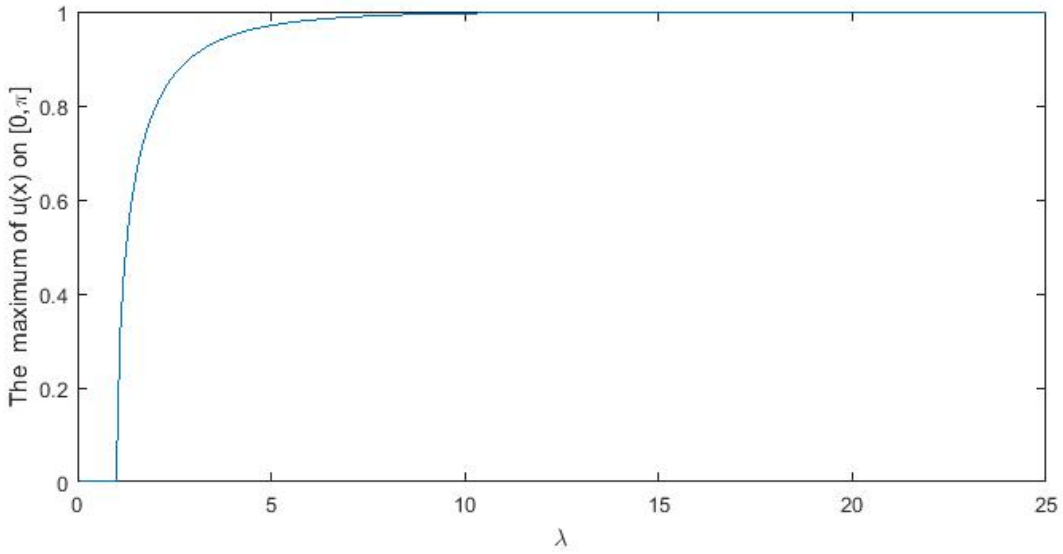

Figure 5.6: The first bifurcation of the nonlocal equation

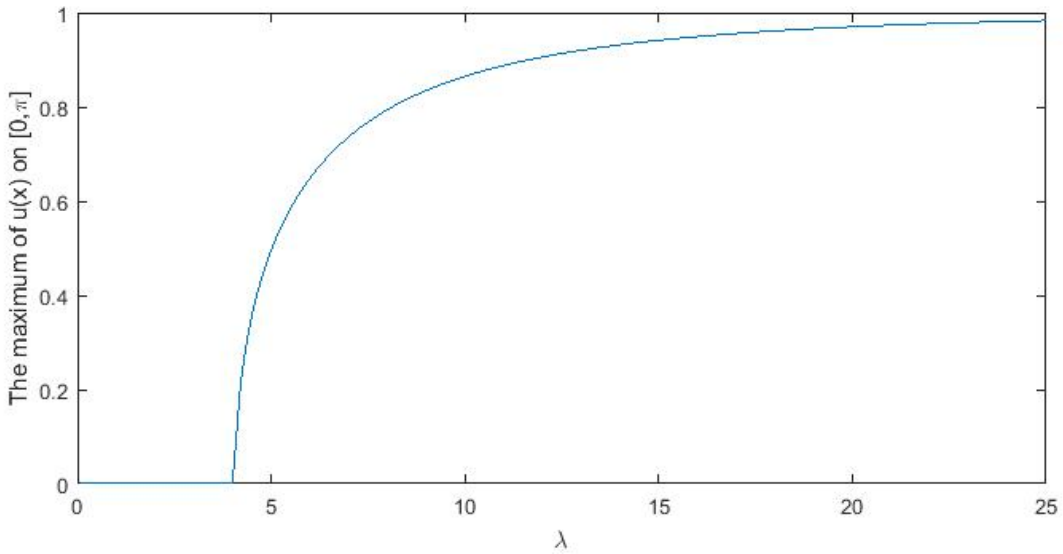

Figure 5.7: The second bifurcation of the nonlocal equation

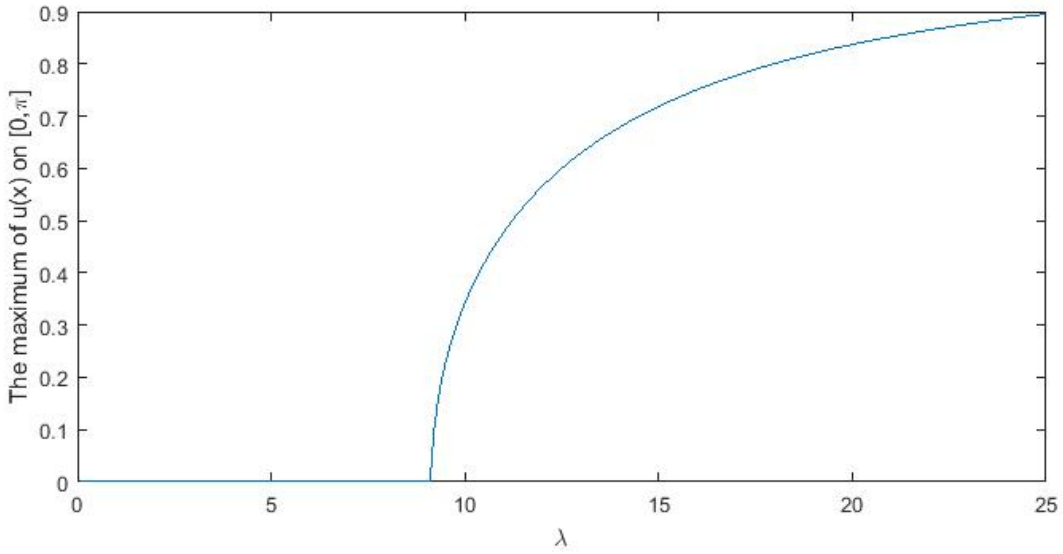

Figure 5.8: The third bifurcation of the nonlocal equation

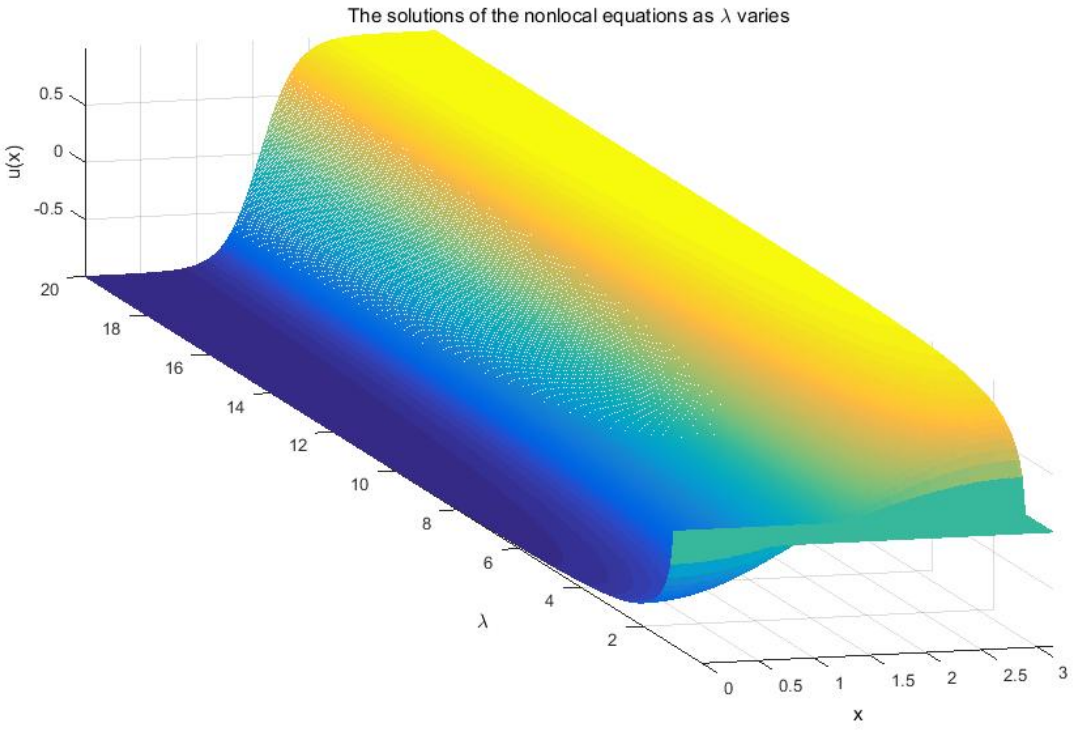

Figure 5.9: The solutions of the nonlocal equation with varying λ

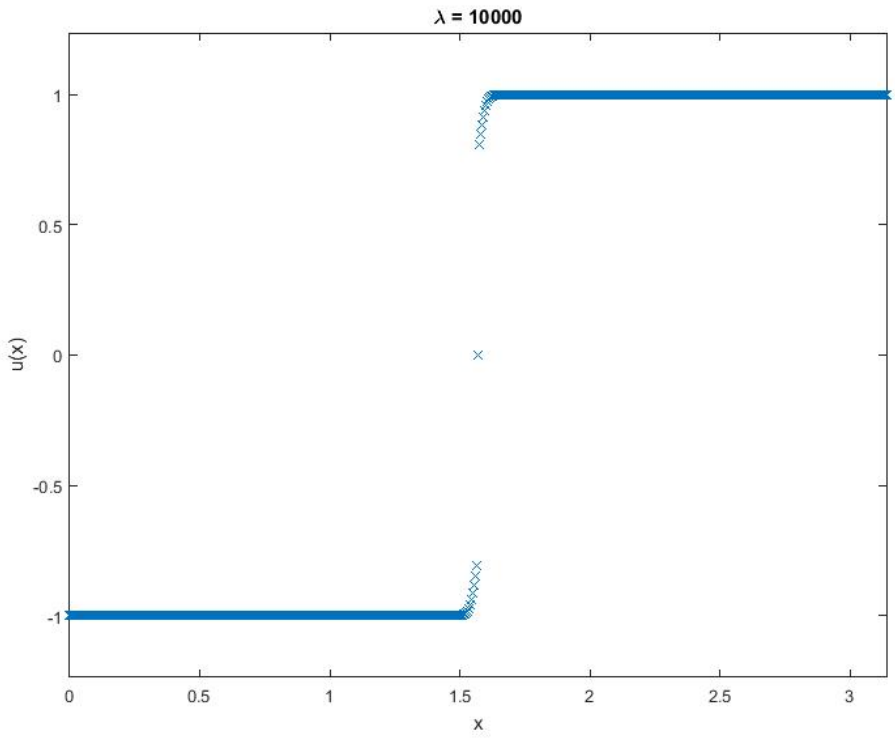

Figure 5.10: The solution of the nonlocal equation the first bifurcation branch when $\lambda = 10000$

BIBLIOGRAPHY

BIBLIOGRAPHY

[1] Erickson RP, Jia Z, Gross SP, Clare CY. *How molecular motors are arranged on a cargo is important for vesicular transport*, PLoS Comput Biol., **7**, 1–22.

[2] Jia Z, Karpeev D, Aranson IS, Bates PW. *Simulation studies of self-organization of microtubules and molecular motors*, Physical Review E., **77(5)** (2008), 051905.

[3] Bates PW, Jia ZH. *Neck-linker tension and the locomotion of kinesin along microtubules*, Can. Appl. Math. Q., (3) (2010), 229–252.

[4] Essaghir A, Dif N, Marbehant CY, Coffer PJ, Demoulin JB. *The transcription of FOXO genes is stimulated by FOXO3 and repressed by growth factors*, J. Biol. Chem., **284** (2009), 10334–10342.

[5] Kops GJ, de Ruiter ND, De Vries-Smits AM, Powell DR, Bos JL, Boudewijn MT. *Direct control of the Forkhead transcription factor AFX by protein kinase B*, Nature, **398** (1999), 630–634.

[6] Matsuzaki H, Daitoku H, Hatta M, Tanaka K, Fukamizu A. *Insulin- induced phosphorylation of FKHR (Foxo1) targets to proteasomal degradation*, Proc. Natl. Acad. Sci. U S A, **100** (2003), 11285–11290.

[7] Puig O, Tjian R. *Transcriptional feedback control of insulin receptor by dFOXO/FOXO1*, Genes & Dev., **19** (2005), 2435–2446.

[8] Quon MJ, Campfield LA. *A mathematical model and computer simulation study of insulin receptor regulation*, J. Theor. Biol., **150** (1991), 59–72.

[9] Quon MJ, Campfield LA. *A mathematical model and computer simulation study of insulin-sensitive glucose transporter regulation*, J. Theor. Biol., **150** (1991), 93–107.

[10] Resino J, Garca-Bellido A. *Drosophila genetic variants that change cell size and rate of proliferation affect cell communication and hence patterning*, Mechanisms of Development, **121** (2004), 351–364.

[11] Sedaghat AR, Sherman A, Quon MJ. *A mathematical model of metabolic insulin signaling pathways*, Am. J. Physiol. Endocrinol. Metab., **283** (2002), 84–101.

[12] Shingleton AW. *The regulation of organ size in Drosophila melanogaster: physiology, plasticity, patterning and physical force*, Organogenesis, **6(2)** (2010), 76–87.

[13] Shingleton AW, Frankino WA, Flatt T, Nijhout HF, Emlen D. *Size and shape: the developmental regulation of static allometry in insects*. BioEssays, textbf29(6) (2007), 536–548.

[14] Smith GR, Shanley DP. *Modelling the response of FOXO transcription factor to multiple post-translational modifications made by ageing-related signalling pathways*, PLoS ONE, **5** (2010), 1–18.

[15] Tang HY, Smith-Caldas MS, Driscoll MV, Salhadar S, Shingleton AW. *FOXO regulates organ-specific phenotypic plasticity in drosophila*, PLoS Genet., **7** (2011), 1–12.

[16] Van Der Heide LP, Hoekman MF, Smidt MP. *The ins and outs of FoxO shuttling: Mechanism of FoxO translocation and transcriptional regulation*, Biochem. J., **380** (2004), 297–309.

[17] Bates PW, Liang Y, Shingleton AW. *Growth regulation and the insulin signaling pathway*, NHM, **8(1)** (2013), 65–78.

[18] Neufeld TP. *Shrinkage control: regulation of insulin-mediated growth by FOXO transcription factors*. J Biol., **2** (2003), 18–54.

[19] Junger MA, Rintelen F, Stocker H, Wasserman JD, Vegh M, et al.. *The Drosophila Forkhead transcription factor FOXO mediates the reduction in cell number associated with reduced insulin signaling*. J Biol., **2** (2003), 20–47.

[20] Kramer JM, Davidge JT, Lockyer JM, Staveley BE. *Expression of Drosophila FOXO regulates growth and can phenocopy starvation*. BMC Dev Biol., **3** (2003), 5–28.

[21] Puig O, Marr MT, Ruhf ML, Tjian R. *Control of cell number by Drosophila FOXO: downstream and feedback regulation of the insulin receptor pathway*. Genes Dev., **17** (2003), 2006–2020.

[22] Van Der Heide LP, Hoekman MF, Smidt MP. *The ins and outs of FoxO shuttling: mechanisms of FoxO translocation and transcriptional regulation*. Biochem J., **380** (2004), 297–309.

[23] Fu W, Ma Q, Chen L, Li P, Zhang M, et al.. *MDM2 acts downstream of p53 as an E3 ligase to promote FOXO ubiquitination and degradation*. J Biol Chem., **284** (2009), 13987–14000.

[24] Kublaoui B, Lee J, Pilch PF. *Dynamics of signaling during insulin-stimulated endocytosis of its receptor in adipocytes*. J Biol Chem., **270** (2009), 59–65.

[25] Madoff DH, Martensen TM, Lane MD. *Insulin and insulin-like growth factor 1 stimulate the phosphorylation on tyrosine of a 160 kDa cytosolic protein in 3T3-L1 adipocytes*. Biochem J., **252** (1988), 7–15.

[26] Bates PW, Zhao G. *Spectral Convergence and Turning Patterns for Nonlocal Diffusion Systems*.

[27] Bates PW, Fife PC, Ren X, Wang X. *Traveling waves in a convolution model for phase transitions*. Archive for Rational Mechanics and Analysis, **138(2)** (1997), 105–136.

[28] Bates PW, Chen X, Chmaj AJ. *Traveling waves of bistable dynamics on a lattice*. SIAM Journal on Mathematical Analysis, **35(2)** (2003), 520–546.

[29] Bates PW, Chen X, Chmaj AJ. *Heteroclinic solutions of a van der Waals model with indefinite nonlocal interactions*. Calculus of Variations and Partial Differential Equations, **24(3)** (2005), 261–281.

[30] Chafee N, Infante EF. *A bifurcation problem for a nonlinear partial differential equation of parabolic type*. Applicable Analysis, **4(1)** (1974), 17–37.

[31] Shi J. *Persistence and bifurcation of degenerate solutions*. Journal of Functional Analysis, **169(2)** (1999), 494–531.

[32] Liu P, Shi J, Wang Y. *Imperfect transcritical and pitchfork bifurcations*. Journal of Functional Analysis, **251(2)** (2007), 573–600.

[33] Crandall MG, Rabinowitz PH. *Bifurcation from Simple Eigenvalues*. Journal of Functional Analysis, **8(2)** (1971), 321–340.

[34] Rabinowitz PH. *Some Global Results for Nonlinear Eigenvalue Problems*. Journal of functional analysis, **7(3)** (1971), 487–513.

[35] Rabinowitz PH. *Some Aspects of Nonlinear Eigenvalue Problems*. Rocky Mountain J. Math, **3(2)** (1973).